People's Democratic Republic of Algeria

Ministry of Higher Education and Scientific Research

University of El Oued

Faculty of Nature and Life Sciences

Department of Cellular and Molecular Biology

MASTER THESIS

In partial fulfilment of the requirements for the degree of Master

Major: Biological Sciences

Speciality: Applied Biochemistry

THEME

Ferrocenyl-Based Acetylaniline Derivatives as Novel DNA Gyrase Inhibitors: Integrated Experimental and Computational Insights for Antibacterial Drug Design

Presented by:

- Zakaria DERKI
- Salah eddine BEN AMOR

Jury Members:

• Dr.	Chaouki DOUIDI	MAA	President
• Dr.	Yacin BOURAS	MAB	Examiner
• Dr.	Elhafnaoui LANEZ	MCA	Supervisor
• Dr.	Housseyn CHAOUA	MAA	Co-Supervisor

Academic Year: 2025 – 2026

Abstract

This thesis presents the design, synthesis, physicochemical characterisation, and comprehensive in silico evaluation of a series of ferrocenyl acetylaniline derivatives (FcMe2Ac, FcMe3Ac, and FcMe4Ac), with particular emphasis on elucidating the relationships between molecular structure, electronic properties, and interaction behaviour toward **bacterial DNA gyrase**, a key enzymatic target in antibacterial drug discovery.

The target compounds were synthesised via a nucleophilic substitution strategy, yielding the desired regioisomers in moderate to high yields (48–80%) with good reproducibility. Structural confirmation was achieved through complementary spectroscopic techniques, including FT-IR, UV–Visible spectroscopy, and one- and two-dimensional NMR analyses. FT-IR spectra displayed characteristic bands corresponding to N–H stretching (~3290–3445 cm^{-1}) and carbonyl functionalities (~1647–1651 cm^{-1}), while UV–Visible spectra revealed absorption maxima in the range of 259–432 nm, attributed to $\pi \rightarrow \pi^*$ transitions within the aromatic system and metal-centred d–d transitions. NMR data confirmed the expected molecular architecture, with distinctive signals corresponding to the ferrocenyl unit (~4.1–4.3 ppm) and aromatic protons (~6.6–7.8 ppm).

Electrochemical characterisation by cyclic voltammetry demonstrated a quasi-reversible Fe(II)/Fe(III) redox process for all derivatives, with formal potentials ranging from 43.9 to 57.5 mV. The observed peak separations (ΔEp = 87.8–115 mV) and near-unity current ratios confirmed quasi-reversible behaviour. Diffusion coefficients (1.11×10^{-7}–5.74×10^{-7} $cm^2 \cdot s^{-1}$) and heterogeneous electron-transfer rate constants (0.14×10^{-3}–0.62×10^{-3} $cm \cdot s^{-1}$) indicated that both transport and kinetic properties are strongly influenced by substitution pattern.

Density functional theory calculations provided detailed insight into the electronic structure, revealing HOMO energies between −5.83 and −5.68 eV and HOMO–LUMO gaps of 3.99–4.29 eV, indicative of moderate chemical stability and controlled reactivity. Global reactivity descriptors confirmed this behaviour, with hardness values ranging from 1.995 to 2.143 eV and electrophilicity indices up to 3.519 eV. The progressive increase in dipole moment (3.82–5.12 D) reflects enhanced molecular polarity across the series.

Molecular docking studies targeting the ATP-binding domain of DNA gyrase (GyrB) demonstrated favourable binding affinities (−7.34 to −8.58 $kcal \cdot mol^{-1}$), with FcMe4Ac exhibiting the strongest interaction. Binding mode analysis revealed stabilisation within the ATP-binding

pocket through hydrophobic interactions, π–π stacking, and hydrogen bonding with key catalytic residues. Molecular dynamics simulations over 100 ns confirmed the stability of the ligand–enzyme complexes, with RMSD values stabilising within ~0.12–0.26 nm and reduced residue fluctuations, indicating a stable and persistent binding mode.

In silico ADMET predictions revealed favourable pharmacokinetic and safety profiles, including high gastrointestinal absorption, balanced lipophilicity (LogP = 3.12–3.45), and absence of predicted mutagenic or hepatotoxic effects. The lack of blood–brain barrier permeability is consistent with a peripheral pharmacokinetic profile, which is advantageous for antibacterial applications.

Overall, the results demonstrate that structural modulation of ferrocenyl derivatives through acetylaniline substitution significantly influences their electronic properties, electrochemical behaviour, and interaction profiles with DNA gyrase. Among the investigated compounds, **FcMe4Ac emerges as the most promising candidate**, combining optimal redox characteristics, strong binding affinity, high dynamic stability, and favourable pharmacokinetic properties, thereby representing a valuable scaffold for the development of novel antibacterial agents.

PART I:

Theoretical Framework

Chapter 1: Theoretical Framework and Scientific Basis for the Study of Ferrocenyl-Based Acetylaniline Derivatives as Novel DNA Gyrase Inhibitors

1.1. General Introduction to the Chapter

Humanity is currently facing a severe global health crisis due to the rapid spread of antibiotic resistance, which threatens the effectiveness of conventional treatments and significantly increases mortality rates associated with both simple and complicated bacterial infections (WHO, 2025; Antimicrobial Resistance Collaborators, 2022). DNA gyrase represents a highly strategic pharmacological target because it is essential for bacterial survival and is absent in eukaryotic cells, thereby offering high selectivity and relatively low toxicity (Collin et al., 2011; Collins & Osheroff, 2024).

This theoretical study aims to provide a comprehensive scientific framework that integrates organometallic chemistry, mechanisms of action of antibacterial agents, the molecular structure of the target enzyme, and modern computational and experimental approaches. The review was conducted through a systematic search of reliable scientific databases including PubMed, Scopus, Web of Science, ScienceDirect, and Google Scholar, with a primary focus on publications from 2015 to 2026 (Dighe et al., 2020; Rajakumari et al., 2024; Bekkar et al., 2025).

1.2. Antibiotic Resistance and the Importance of Discovering New Compounds

Bacterial resistance mechanisms have evolved through multiple major pathways, including target modification, drug efflux pumps, production of drug-degrading enzymes such as β-lactamases, and the formation of protective biofilms (Sun et al., 2025; Kherroubi et al., 2024). The ESKAPE pathogens (*Enterococcus faecium*, *Staphylococcus aureus*, *Klebsiella pneumoniae*, *Acinetobacter baumannii*, *Pseudomonas aeruginosa*, and *Enterobacter* spp.) constitute the greatest global threat due to their multidrug-resistant (MDR) profiles.

The overuse of fluoroquinolones has led to the widespread emergence of mutations in the quinolone resistance-determining regions (QRDR) of the *gyrA* and *parC* genes (Aldred et al.,

2014; Collin et al., 2011). Consequently, the development of novel DNA gyrase inhibitors with structurally distinct scaffolds, particularly organometallic hybrid compounds, has become an urgent priority to overcome existing resistance and address the global need for new antibacterial agents (Alfonso et al., 2022; Bekkar et al., 2025; Bakker et al., 2024).

1.3. DNA Gyrase: Structure, Function, and Mechanism of Action

DNA gyrase is a Type II topoisomerase found exclusively in bacteria. It consists of two main subunits: GyrA, responsible for DNA cleavage and religation, and GyrB, which contains the ATPase domain. The functional enzyme exists as a heterotetramer of the A_2B_2 type (Collins & Osheroff, 2024; Fukuda et al., 2026).

The catalytic mechanism of DNA gyrase involves a complex multi-step cycle. Initially, the enzyme binds to DNA and introduces a positive node using the C-terminal domain of GyrA. Two ATP molecules then bind to the N-terminal domain of GyrB, inducing dimerization of the ATPase domains and closing the N-gate. The transported DNA segment (T-segment) is captured within the cavity. Subsequently, GyrA performs double-strand cleavage of the gate segment (G-segment) through a nucleophilic attack by tyrosine residues, forming covalent phosphotyrosine bonds. The T-segment is passed through the double-strand break, followed by religation of the G-segment facilitated by magnesium ions. Finally, ATP hydrolysis in GyrB provides the energy required to introduce approximately two negative supercoils per cycle, thereby relieving the positive torsional stress generated ahead of the replication fork (Champoux, 2001; Collin et al., 2011; Fukuda et al., 2026; Vayssières et al., 2024).

This mechanism differs from that of Topoisomerase IV, which primarily performs decatenation, and from human Topoisomerase IIα, conferring significant drug selectivity to bacterial DNA gyrase (Collins & Osheroff, 2024).

1.4. Current DNA Gyrase Inhibitors and Their Mechanisms of Action

DNA gyrase inhibitors are broadly classified into two main categories.

DNA Gyrase Poisons (e.g., Fluoroquinolones): Fluoroquinolones such as ciprofloxacin bind at two sites near the cleavage core in GyrA and stabilize the enzyme-DNA-drug ternary complex in a cleaved state. This prevents religation of the broken DNA strands, leading to double-strand breaks when replication or transcription forks collide with the stabilized complex. The resulting DNA damage activates the SOS response and ultimately causes bacterial cell death. The binding relies on a water-metal ion bridge (Mg^{2+}) interacting with residues such as Ser83 and Asp87 in GyrA. Mutations in the QRDR reduce this interaction and confer resistance (Aldred et al., 2014; Spencer et al., 2023; Fukuda et al., 2026).

Competitive ATP Inhibitors (e.g., Aminocoumarins such as Novobiocin): These compounds bind directly to the ATP-binding site in the N-terminal domain of GyrB, competitively inhibiting ATP binding and depriving the enzyme of the energy required for supercoiling without causing DNA breakage (Maxwell & Lawson, 2003; Fukuda et al., 2026).

Newer classes include Novel Bacterial Topoisomerase Inhibitors (NBTIs) such as gepotidacin, which bind at a central site (site S2) and stabilize DNA in a closed conformation, and allosteric inhibitors such as isoquinoline sulfonamides, which bind to distant hydrophobic pockets and induce conformational changes that impair enzyme function (Gedeon et al., 2024; Bakker et al., 2024; Alfonso et al., 2022).

1.5. Organometallic Chemistry and Ferrocene in Drug Design

Ferrocene ($C_{10}H_{10}Fe$) is a stable organometallic compound characterized by unique redox properties (reversible Fe^{2+}/Fe^{3+} transition), high lipophilicity, and relatively low toxicity (Hassan et al., 2018; Sharma et al., 2021). It has been successfully incorporated into hybrid drugs such as ferroquine (antimalarial) and ferrocifen (anticancer), where it improves bioavailability, metabolic stability, and introduces additional mechanisms such as the generation of reactive oxygen species (ROS) (Dive & Biot, 2008; Ornelas et al., 2023).

In the antibacterial field, ferrocene derivatives enhance activity by improving cell membrane penetration, facilitating DNA binding, and disrupting cellular redox balance through electrochemical interactions (Hassan et al., 2018; Bekkar et al., 2025; Khurshid et al., 2026).

1.6. Acetylaniline Derivatives and Their Pharmaceutical Applications

Acetanilide serves as an important chemical scaffold for numerous drugs, most notably paracetamol (acetaminophen). Its derivatives are characterized by their ability to form strong hydrogen bonds and π-π stacking interactions with biological targets (Magri et al., 2016; Sheikh et al., 2023). Modifications on the nitrogen atom (N-substitution) or the aromatic ring can significantly improve antibacterial activity, DNA binding affinity, and selectivity (Abd Halim et al., 2024). N-acetylation further enhances both chemical and biological stability.

1.7. Ferrocenyl-Acetylaniline Hybrid Compounds: Design and Previous Studies

N-ferrocenylmethyl-N-acetylaniline (FMAA) derivatives and their analogs (FMA and FMBA) represent promising hybrid scaffolds. These compounds have demonstrated potent antibacterial activity against *E. coli*, *S. aureus*, and *P. aeruginosa*, with low MIC and IC_{50} values (Bekkar et al., 2025). Electrochemical and spectroscopic studies revealed strong electrostatic and minor groove binding interactions with DNA, particularly in G/C-rich regions (Yahiaoui et al., 2024). This hybrid design combines the redox properties of ferrocene with the hydrogen-bonding capability of the acetylaniline moiety, effectively addressing issues of resistance and selectivity (Bekkar et al., 2025; Hassan et al., 2018).

1.8. Computational Methods in Inhibitor Design and Development

Computational approaches provide an integrated strategy for predicting activity, stability, and drug-like properties.

Molecular Docking employs search algorithms in software such as AutoDock Vina or Glide to predict binding poses and binding free energy (ΔG) between the ligand and the target (GyrA or GyrB). It evaluates non-covalent interactions including hydrogen bonds, hydrophobic contacts, π-π stacking, and electrostatic forces. In FMAA/FMBA derivatives, docking studies indicated strong binding near the ATP site or in the minor groove (Bekkar et al., 2025; Kumar et al., 2023).

Molecular Dynamics (MD) Simulations use packages such as GROMACS or AMBER to simulate atomic movements over 50–300 ns in an aqueous environment. Key parameters analyzed include RMSD (structural stability), RMSF (residue flexibility), hydrogen bond persistence, and binding free energy calculated via MM-PBSA/GBSA methods. These simulations confirm the long-term stability of ligand-enzyme-DNA complexes (Bekkar et al., 2025; Moulishankar et al., 2024).

Density Functional Theory (DFT) Calculations (typically B3LYP/6-311++G(d,p)) evaluate electronic properties such as HOMO and LUMO energies, energy gap (ΔE — smaller gap indicates higher reactivity), Molecular Electrostatic Potential (MEP) maps for identifying nucleophilic/electrophilic sites, and global reactivity descriptors (chemical hardness, softness, and electrophilicity index). These calculations help explain the redox behavior of the ferrocenyl moiety (Bekkar et al., 2025; Tabrizi et al., 2020).

Complementary tools include pharmacophore modeling, QSAR, and ADMET predictions (SwissADME, pkCSM) to assess compliance with Lipinski's rule of five and overall drug-likeness (Moulishankar et al., 2024).

1.9. Experimental Techniques for Evaluating DNA Gyrase Inhibitors and DNA Binding

Experimental evaluation includes antibacterial susceptibility tests (MIC, MBC, disk diffusion), enzyme inhibition assays (supercoiling assay and ATPase assay), and DNA interaction studies using UV-Vis spectroscopy, fluorescence quenching, circular dichroism, viscosity measurements, and cyclic voltammetry. Structural characterization is performed using NMR, IR, MS, and XRD techniques (Alfonso et al., 2022; Yahiaoui et al., 2024; Bekkar et al., 2025).

1.10. Integrated Approaches and Future Perspectives

The integrated experimental-computational approach provides precise mechanistic insights and accelerates drug discovery (Bekkar et al., 2025; Collins & Osheroff, 2024). Major challenges include toxicity, metabolic stability, and bioavailability, while opportunities lie in structural

optimization for targeting resistant strains and achieving selective ROS generation within bacterial cells.

1.11. General Conclusion of the Chapter

The hybridization of ferrocene with acetylaniline derivatives represents an innovative and promising strategy for developing new DNA gyrase inhibitors effective against antibiotic-resistant bacteria. This theoretical framework establishes a solid scientific foundation for the experimental and computational sections of the thesis (Hassan et al., 2018; Bekkar et al., 2025; Collins & Osheroff, 2024; WHO, 2025).

PART II:

EXPERIMENTAL

Chapter 01:

Materials & Methods

1. General Introduction

This chapter outlines the experimental protocols and computational strategies adopted for the synthesis, structural elucidation, and in silico investigation of ferrocenyl acetylaniline derivatives. The overall methodology integrates synthetic organometallic chemistry with advanced spectroscopic, electrochemical, and molecular modelling techniques in order to establish a comprehensive correlation between molecular structure, electronic properties, and interaction behaviour toward **bacterial DNA gyrase**, a key enzymatic target in antibacterial drug discovery.

The synthesis of the target compounds was carried out at the Laboratory of Valorisation and Technology of Saharian Resources (VTRS), Faculty of Technology, University of El Oued, under controlled laboratory conditions. The same research facility was used to perform all computational investigations, including density functional theory (DFT) calculations, molecular docking, molecular dynamics simulations, and MM-PBSA analyses, thereby ensuring methodological consistency between experimental and theoretical results.

Spectroscopic characterisation was conducted in collaboration with the Centre de Recherche Scientifique et Technique en Analyses Physico-Chimiques (CRAPC), University of Ouargla. A combination of FT-IR, UV–Visible spectroscopy, and one- and two-dimensional NMR techniques was employed to confirm the molecular structures of the synthesised derivatives. In addition, cyclic voltammetry was used to explore the redox properties of the ferrocenyl core, which are directly related to its electronic behaviour and may influence its interaction with biological targets.

Particular emphasis was placed on evaluating the interaction potential of these compounds with **bacterial DNA gyrase (GyrB ATP-binding domain)**, an essential type II topoisomerase responsible for DNA supercoiling and replication in bacteria, and a validated target for antibacterial therapy. To this end, molecular docking and molecular dynamics simulations were performed to investigate binding affinity, interaction mechanisms, and structural stability of the ligand–enzyme complexes.

Furthermore, in silico ADMET predictions were carried out to assess pharmacokinetic properties, drug-likeness, and potential toxicity, providing a preliminary evaluation of their suitability as antibacterial agents.

Overall, this integrated approach ensures the robustness and reliability of the obtained data and provides a solid framework for understanding the physicochemical behaviour and biological relevance of ferrocenyl derivatives in the context of antibacterial drug design.

2. Chemicals and Reagents

All reagents and solvents employed in this study were of analytical grade and used without further purification unless otherwise specified. The choice of chemicals was guided by their suitability for organometallic synthesis and compatibility with subsequent spectroscopic, electrochemical, and computational analyses.

Ferrocene (Fc, 99%) and orthophosphoric acid (85%) were supplied by Alfa Aesar. The o-, m-, and p-aminoacetophenone isomers (99%), along with tetrabutylammonium tetrafluoroborate (Bu_4NBF_4, electrochemical grade, 99%) used as supporting electrolyte, were obtained from Sigma-Aldrich. Iodomethane and anhydrous magnesium sulfate (97%) were purchased from Acros Organics, while acetic acid (99–100%) and ethanol (95%) were provided by Biochem Chemopharma.

The ferrocenylmethyl quaternary ammonium intermediate was synthesised according to previously reported procedures and used directly without additional purification [1]. All aqueous solutions were prepared using double-distilled water, and solvents used for analytical and electrochemical measurements were of appropriate purity to ensure reproducibility.

Stock solutions were freshly prepared when required and handled under standard laboratory conditions to minimise degradation and contamination.

3. Instrumentation and Experimental Conditions

3.1. Spectroscopic Analysis

3.1.1. FT-IR Spectroscopy

Fourier-transform infrared (FT-IR) spectra were recorded using a Shimadzu 8000S spectrophotometer over the range 4000–400 cm^{-1}. Solid samples were prepared as KBr pellets.

This technique enabled identification of key functional groups, including N–H stretching, carbonyl (C=O) vibrations and aromatic C–H bonds, thereby confirming the formation of the ferrocenyl acetylaniline framework [1].

3.1.2. UV–Visible Spectroscopy

Electronic absorption spectra were obtained using a Shimadzu UV-1800 spectrophotometer in the range 200–900 nm. Measurements were carried out in dimethyl sulfoxide (DMSO) using quartz cuvettes (1 cm path length).

The analysis provided information on electronic transitions within the molecules, including π–π*, n–π* and metal-centred transitions, reflecting the conjugation between the ferrocenyl unit and the aromatic system [2].

3.2. Nuclear Magnetic Resonance (NMR)

3.2.1. ^{1}H NMR Analysis

^{1}H NMR spectra were recorded on a Bruker ARX-500 spectrometer (400 MHz) using DMSO-d_6 as solvent. Chemical shifts (δ) were referenced to tetramethylsilane (TMS).

The spectra allowed clear identification of proton environments associated with the ferrocenyl rings, aromatic moiety, methylene bridge and acetyl group, confirming the expected molecular structures [3].

3.2.2. ^{13}C NMR Analysis

^{13}C NMR spectra were obtained under similar experimental conditions. The analysis provided detailed assignment of carbon atoms, including carbonyl carbons, aromatic carbons, cyclopentadienyl rings and methylene carbons.

These data confirmed the successful functionalisation of the ferrocenyl scaffold [4].

3.2.3. Two-Dimensional NMR (HSQC/HMBC)

Two-dimensional NMR experiments (HSQC and HMBC) were performed to establish proton–carbon correlations.

HSQC enabled direct one-bond correlations, while HMBC provided long-range connectivity, allowing unambiguous structural assignment and confirmation of substitution patterns on the aromatic ring [5].

3.3. Electrochemical Measurements (Cyclic Voltammetry)

Electrochemical measurements were carried out using a PGZ301 potentiostat/galvanostat (Radiometer Analytical, France) in dimethyl sulfoxide (DMSO) under nitrogen atmosphere at 298 K.

A conventional three-electrode system was employed, consisting of a glassy carbon working electrode (0.013 cm^2), a platinum counter electrode (0.05 cm^2) and a saturated Hg/Hg_2Cl_2 reference electrode. Tetrabutylammonium tetrafluoroborate (0.1 M) was used as supporting electrolyte.

Prior to each experiment, the solution was purged with nitrogen to eliminate dissolved oxygen and ensure stable electrochemical conditions.

Cyclic voltammetry measurements were performed within a defined potential window to investigate the Fe(II)/Fe(III) redox behaviour of the ferrocenyl derivatives. The obtained electrochemical parameters provided insight into electron-transfer processes and the intrinsic electronic properties of the compounds [6].

4. Synthesis of Ferrocenyl Acetylaniline Derivatives

This section outlines the synthetic route adopted for the preparation of the ferrocenyl acetylaniline derivatives. The methodology is based on a nucleophilic substitution strategy involving a ferrocenylmethyl quaternary ammonium intermediate, allowing efficient formation of the C–N bond under relatively mild reaction conditions. This approach ensures good selectivity, operational simplicity and reproducibility in obtaining the three regioisomeric derivatives.

The overall synthetic pathway is illustrated in Figure 1, which depicts the generation of the ferrocenylmethyl intermediate followed by its coupling with the corresponding aminoacetophenone isomers.

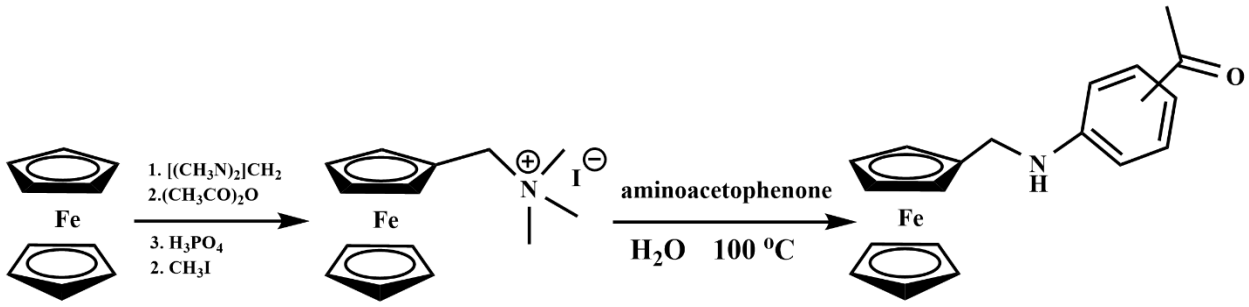

Figure 1. Synthetic route for the preparation of N-[(ferrocenyl)methyl]acetylaniline derivatives (FcMe2Ac, FcMe3Ac and FcMe4Ac).

4.1. General Synthetic Procedure

The target compounds were synthesised via nucleophilic substitution between trimethylferrocenylmethylammonium iodide and the corresponding aminoacetophenone isomers (ortho, meta and para), as shown in Figure 1.

In a typical experiment, the selected aminoacetophenone (3.84 mmol) was progressively introduced into a stirred aqueous solution of trimethylferrocenylmethylammonium iodide (2.56 mmol) dissolved in distilled water (60 mL). The reaction mixture was maintained under reflux for 4 hours to ensure complete conversion.

After completion, the mixture was cooled to ambient temperature, resulting in the formation of a yellow precipitate. The crude product was recovered by vacuum filtration and washed thoroughly with distilled water to eliminate residual salts and unreacted reagents.

Purification was achieved by recrystallisation from a 90% ethanol/water mixture. For the meta-substituted derivative, an additional purification step using column chromatography (chloroform/methanol, 99:1 v/v) was required to obtain a higher purity product.

This synthetic protocol offers several advantages, including the use of an aqueous medium, straightforward experimental handling and avoidance of harsh conditions, making it well-suited for the reproducible synthesis of ferrocenyl derivatives [7].

4.2. Synthesis of Individual Compounds

4.2.1. N-[(ferrocenyl)methyl]-2-acetylaniline (FcMe2Ac)

Yield: 650 mg (77%).

Appearance: Yellow crystalline solid.

Melting point: 148–150 °C.

^{1}H NMR (500 MHz, DMSO-d_6): δ 2.60 (3H, m, CH_3), 3.40 (2H, t, α-C_5H_4), 4.05 (2H, t, β-C_5H_4), 4.15 (5H, s, C_5H_5), 4.30 (2H, d, CH_2N), 6.62 (1H, m, Ar-H), 6.84 (1H, d, Ar-H), 7.40 (1H, m, Ar-H), 7.85 (1H, d, Ar-H), 9.01 (1H, s, NH).

^{13}C NMR (500 MHz, DMSO-d_6): δ 29 (CH_3), 42 (CH_2N), 67, 68 (C_5H_4), 69 (C_5H_5), 87 (ipso-C), 112, 116, 118, 134, 138, 150 (aromatic carbons), 210 (C=O).

FT-IR (KBr, ν, cm^{-1}): 3426, 3291 (N–H), 3082 (Ar–C–H), 1647 (C=O), 1566, 1516 (C=C), 1454, 1416, 1146, 1003, 617.

UV–Vis (DMSO): λmax = 259 nm (π–π*), 380 nm (d–d).

Cyclic voltammetry (DMSO, Fc^+/Fc): Ipa = 29.13 μA, Ipc = −28.52 μA, Epa = 2.17 mV, Epc = −85.60 mV, ΔE = 87.8 mV, E° = 43.9 mV, Ipa/Ipc = 1.02.

4.2.2. N-[(ferrocenyl)methyl]-3-acetylaniline (FcMe3Ac)

Yield: 480 mg (48%).

Appearance: Yellow–orange crystalline solid.

Melting point: 138–140 °C.

^{1}H NMR (500 MHz, DMSO-d_6): δ 2.45 (3H, s, CH_3), 3.42 (2H, t, α-C_5H_4), 4.08 (2H, t, β-C_5H_4), 4.18 (5H, s, C_5H_5), 4.32 (2H, d, CH_2N), 6.70–7.20 (3H, m, Ar-H), 7.65 (1H, d, Ar-H), 8.95 (1H, s, NH).

^{13}C NMR (500 MHz, DMSO-d_6): δ 28 (CH_3), 43 (CH_2N), 66, 68 (C_5H_4), 69 (C_5H_5), 86 (ipso-C), 114, 118, 125, 131, 136, 152 (aromatic carbons), 205 (C=O).

FT-IR (KBr, ν, cm^{-1}): 3432, 3338 (N–H), 2925, 1650 (C=O), 1582, 1510, 1450, 1365, 1170, 820.

UV–Vis (DMSO): λmax = 268 nm, 402 nm.

Cyclic voltammetry (DMSO, Fc^+/Fc): Ipa = 52.4 μA, Ipc = −51.9 μA, Epa = 10 mV, Epc = −92 mV, ΔE = 102 mV, E° = 51.0 mV, Ipa/Ipc = 1.01.

4.2.3. N-[(ferrocenyl)methyl]-4-acetylaniline (FcMe4Ac)

Yield: 690 mg (80%).

Appearance: Deep yellow crystalline solid.

Melting point: 162–164 °C.

^{1}H NMR (500 MHz, DMSO-d_6): δ 2.35 (3H, m, CH_3), 3.41 (2H, t, α-C_5H_4), 4.10 (2H, t, β-C_5H_4), 4.20 (5H, s, C_5H_5), 4.31 (2H, d, CH_2N), 6.65 (2H, d, Ar-H), 6.78 (1H, t, NH), 7.76 (2H, d, Ar-H).

^{13}C NMR (500 MHz, DMSO-d_6): δ 28 (CH_3), 43 (CH_2N), 66 (C_5H_4), 68 (C_5H_5), 87 (ipso-C), 112, 125, 132, 154 (aromatic carbons), 194 (C=O).

FT-IR (KBr, ν, cm^{-1}): 3445, 3345 (N–H), 2932, 1651 (C=O), 1589, 1562, 1369, 1281, 1173, 822.

UV–Vis (DMSO): λmax = 432 nm.

Cyclic voltammetry (DMSO, Fc^+/Fc): Ipa = 71.07 μA, Ipc = −71.66 μA, Epa = 16 mV, Epc = −99 mV, ΔE = 115 mV, E° = 57.5 mV, Ipa/Ipc = 0.99.

5. Computational Methodology

Computational analyses were undertaken to elucidate the electronic characteristics and interaction potential of the synthesised ferrocenyl acetylaniline derivatives in relation to their

inhibitory activity against **bacterial DNA gyrase (GyrB ATP-binding domain)**, a key enzyme involved in DNA supercoiling and replication and a validated target in antibacterial drug development.

The adopted in silico framework integrates density functional theory (DFT), molecular docking, molecular dynamics (MD) simulations, and MM-PBSA binding free energy calculations, complemented by ADMET prediction tools.

This integrated methodology enables the establishment of correlations between molecular structure, electronic distribution, and binding behaviour toward DNA gyrase, thereby providing mechanistic insight into ligand–enzyme recognition and inhibition potential at the molecular level.

5.1. Electronic Structure Calculations (DFT)

Quantum chemical calculations were performed using Gaussian 16 [8] to investigate the electronic properties of FcMe2Ac, FcMe3Ac, and FcMe4Ac.

Geometry optimisation was carried out at the B3LYP level using the 6-311++G(d,p) basis set for light atoms (C, H, N, O), while the Stuttgart–Dresden (SDD) effective core potential was applied to the iron centre [9]. Vibrational frequency calculations were performed at the same level of theory to confirm that all optimised structures correspond to true minima on the potential energy surface, as evidenced by the absence of imaginary frequencies.

The optimised geometries were subsequently used to evaluate frontier molecular orbitals (HOMO and LUMO), energy gaps, and global reactivity descriptors, including electronegativity, chemical hardness, softness, and electrophilicity index. These parameters provide valuable insight into the intrinsic reactivity of the compounds and their ability to participate in charge transfer interactions with the ATP-binding site of DNA gyrase.

In addition, molecular electrostatic potential (MEP), electron localisation function (ELF), localised orbital locator (LOL), and reduced density gradient (RDG) analyses were performed to characterise charge distribution, electron delocalisation, and weak non-covalent interactions. These analyses are particularly relevant for understanding the nature of ligand–enzyme interactions, including hydrogen bonding, van der Waals forces, and π-related interactions within the DNA gyrase binding pocket.

Visualisation and analysis of the computed properties were carried out using GaussView and Multiwfn [10].

5.2. Molecular Docking Simulations

Molecular docking studies were conducted to evaluate the binding affinity and interaction mechanisms of the ferrocenyl acetylaniline derivatives with **bacterial DNA gyrase (GyrB ATP-binding domain)**, a key enzyme responsible for DNA supercoiling and replication in bacteria and a validated target for antibacterial drug development.

The crystallographic structure used in this study was **PDB ID: 6RKS**, corresponding to the ATP-binding domain of DNA gyrase B co-crystallised with a known inhibitor, providing a reliable structural model for analysing ligand binding within the catalytic pocket.

5.2.1. Receptor Preparation

The three-dimensional structure of the selected DNA gyrase target is illustrated in Figure 2, highlighting the organisation of the ATP-binding site and key residues involved in ligand recognition.

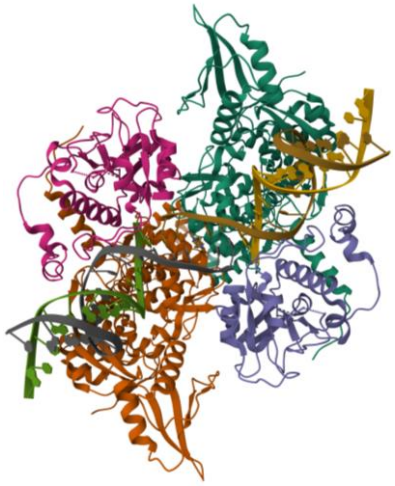

Figure 2. Three-dimensional structure of bacterial DNA gyrase B (GyrB ATP-binding domain) used in docking studies (PDB ID: 6RKS).

The crystallographic structures were retrieved from the Protein Data Bank (https://www.rcsb.org/) [11] and prepared using AutoDock Tools (ADT 1.5.7) [12]. All crystallographic water molecules, co-crystallised ligands, and non-essential heteroatoms were removed to avoid interference with ligand binding. Polar hydrogen atoms were added, and Kollman charges were assigned. The prepared receptors were then converted into PDBQT format.

5.2.2. Ligand Preparation

The optimised geometries of FcMe2Ac, FcMe3Ac, and FcMe4Ac were used as input structures (Figure 3).

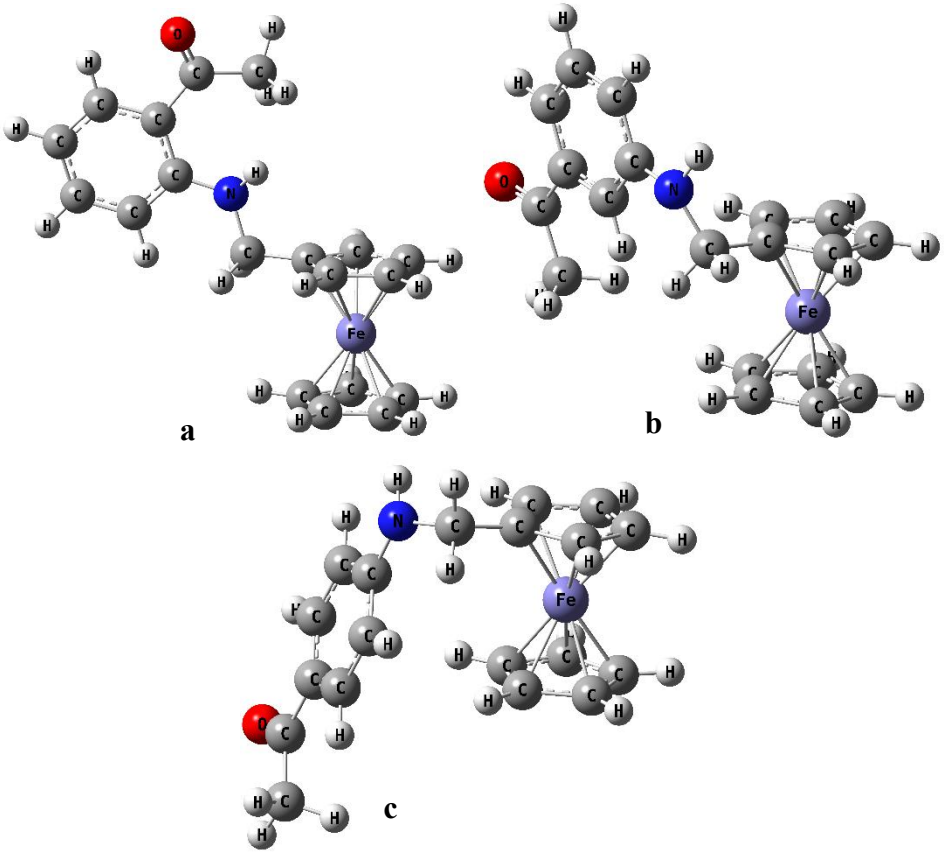

Figure 3. Optimised molecular structures of ferrocenyl derivatives used as ligands: FcMe2Ac (a), FcMe3Ac (b), and FcMe4Ac (c).

Ligands were prepared using AutoDock Tools by assigning Gasteiger charges and defining rotatable bonds, followed by conversion into PDBQT format.

5.2.3. Docking Protocol and Validation

The docking workflow is presented in Figure 4, summarising receptor preparation, ligand preparation, grid generation and docking analysis.

c

a **b**

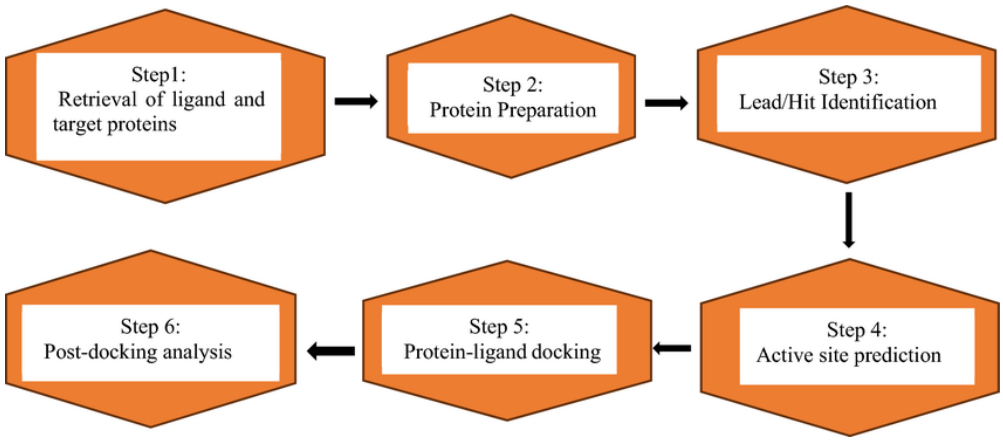

Figure 4. Molecular docking workflow illustrating protein and ligand preparation, grid generation, docking execution and interaction analysis.

Docking simulations were performed using AutoDock 4.2 employing the Lamarckian genetic algorithm. A grid box of **60 × 60 × 60 Å** with a spacing of **0.375 Å** was centred on the **ATP-binding pocket of DNA gyrase (GyrB)**, which represents the primary site for inhibitor binding and enzymatic activity regulation.

A total of **100 independent docking runs** were performed for each ligand–target system to ensure adequate conformational sampling. The most stable binding pose was selected based on the lowest binding energy and the highest cluster population.

Validation of the docking protocol was carried out by **redocking the co-crystallised ligand** into the ATP-binding site of DNA gyrase and calculating the root-mean-square deviation (RMSD) between the experimental and predicted conformations. An RMSD value below **2.0 Å** confirmed the reliability and accuracy of the docking setup, ensuring its suitability for predicting ligand–enzyme interactions [13].

5.3. Molecular Dynamics (MD) Simulations

Molecular dynamics (MD) simulations were carried out to evaluate the stability and dynamic behaviour of the selected ligand–**DNA gyrase (GyrB)** complexes using GROMACS [15]. This approach allows a detailed investigation of the temporal evolution of ligand–enzyme interactions within the **ATP-binding domain**, providing insight into the stability and persistence of binding under simulated physiological conditions [14].

5.3.1. System Setup and Solvation

The solvated system is illustrated in Figure 5, showing the protein–DNA–ligand complex embedded in an explicit water box.

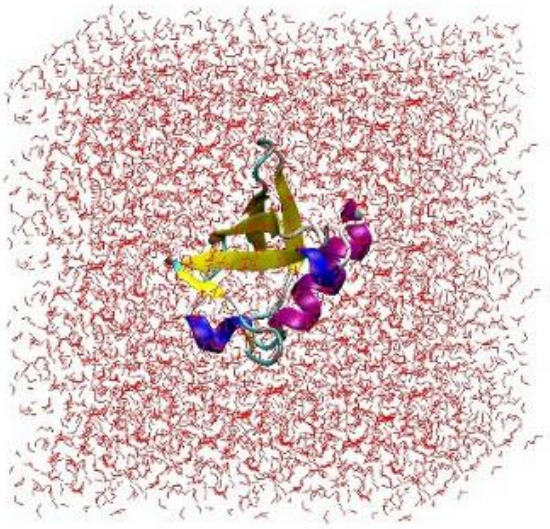

Figure 5. Solvated protein–ligand complex showing the explicit water box used for molecular dynamics simulations.

The CHARMM36 force field was employed for protein parameterisation [15], while ligand parameters were generated using the CGenFF protocol [16]. Each system was placed in a cubic simulation box with a minimum distance of 10 Å between the protein surface and the box boundary and solvated using the TIP3P water model. Counter ions were added to neutralise the system and ensure electrostatic stability.

5.3.2. Energy Minimisation and Equilibration

The general molecular dynamics simulation protocol, including minimisation, equilibration, and production stages, is summarised in Figure 6.

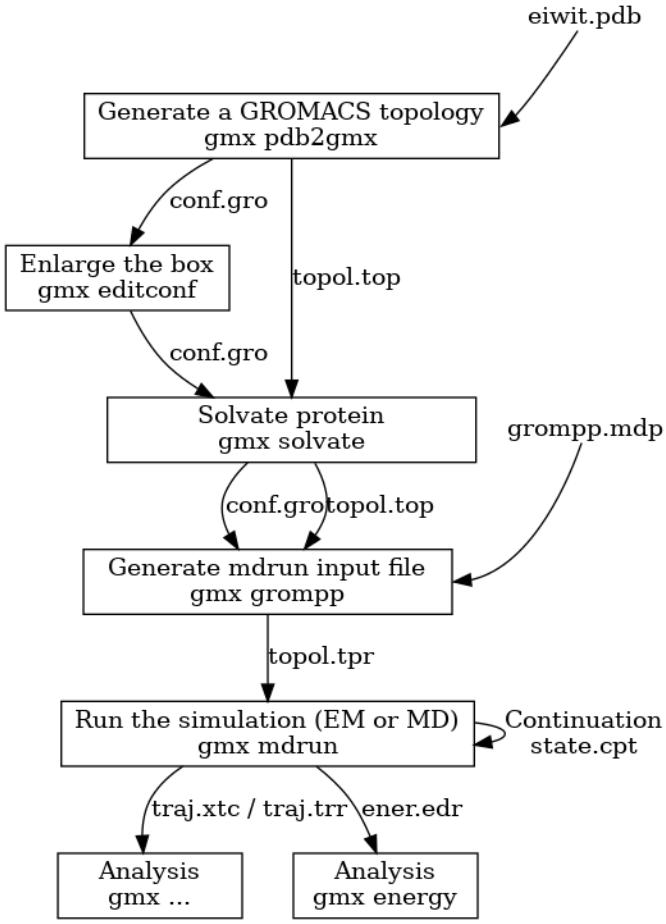

Figure 6. Molecular dynamics simulation workflow including system preparation, energy minimisation, equilibration and production phases.

Energy minimisation was performed using the steepest descent algorithm to eliminate steric clashes and optimise the system geometry. The system was subsequently equilibrated under NVT conditions (300 K, 500 ps), followed by NPT conditions (1 atm, 500 ps), using the V-rescale thermostat and Parrinello–Rahman barostat.

5.3.3. Production Run Parameters

Production simulations were conducted for 100 ns with a time step of 2 fs. Periodic boundary conditions were applied in all directions, and long-range electrostatic interactions were treated using the Particle Mesh Ewald (PME) method. Covalent bonds involving hydrogen atoms were constrained using the LINCS algorithm.

Trajectory analyses were carried out using GROMACS built-in tools, including RMSD, RMSF, radius of gyration (Rg), and solvent surface accessibility area (SASA).

5.4. MM-PBSA Binding Free Energy Calculations

Binding free energy calculations were performed using the g_mmpbsa tool [17]. Snapshots extracted from the last 20 ns of equilibrated trajectories were used.

The total binding free energy (ΔG_bind) was estimated as the sum of van der Waals, electrostatic, polar solvation and non-polar solvation contributions.

5.5. ADMET Prediction

Pharmacokinetic and toxicity properties were predicted using ADMETlab 2.0 [18] and ProTox-II [19] to evaluate the suitability of the synthesised compounds as potential **antibacterial agents**.

Key parameters assessed included gastrointestinal absorption, lipophilicity, cytochrome P450 interactions, plasma protein binding, and toxicity indicators such as hepatotoxicity, mutagenicity, and LD_{50}.

These predictions provide an initial evaluation of drug-likeness, bioavailability, and safety, which are essential for the development of compounds targeting bacterial enzymes such as DNA gyrase.

Chapter 02:

Results & Discussion

1. General Introduction

This chapter presents a comprehensive analysis of the experimental and computational results obtained for the synthesised ferrocenyl acetylaniline derivatives. The primary objective is to establish clear correlations between molecular structure, electronic properties, and their interaction behaviour toward **bacterial DNA gyrase (GyrB ATP-binding domain)**, a key enzymatic target in antibacterial drug development.

The discussion begins with an evaluation of the synthetic outcomes, including reaction efficiency, yield optimisation, and the influence of substitution patterns on the physicochemical properties of the obtained derivatives. This is followed by an in-depth structural characterisation using FT-IR, UV–visible spectroscopy, nuclear magnetic resonance (^{1}H, ^{13}C, and 2D NMR), and cyclic voltammetry. These complementary techniques provide robust confirmation of molecular structures and offer valuable insight into the electronic behaviour of the ferrocenyl core, which plays a crucial role in modulating redox properties and interaction potential.

Subsequently, computational investigations are presented to extend and rationalise the experimental findings. Density functional theory calculations are employed to analyse electronic descriptors, charge distribution, and reactivity parameters, providing a molecular-level understanding of the intrinsic properties of the compounds.

Molecular docking and molecular dynamics simulations are then utilised to explore the interaction of the synthesised derivatives with the **ATP-binding pocket of DNA gyrase**, with particular emphasis on binding affinity, interaction mechanisms, and dynamic stability of the ligand–enzyme complexes. These analyses provide detailed insight into the molecular recognition process and the structural factors governing binding efficiency.

Finally, MM-PBSA binding free energy calculations and ADMET predictions are discussed to evaluate interaction stability, energetic favourability, and pharmacokinetic suitability of the compounds as potential antibacterial agents.

Overall, this integrated analysis provides a comprehensive understanding of the structure–property–interaction relationships governing ferrocenyl acetylaniline derivatives and highlights their potential as promising scaffolds for targeting bacterial DNA gyrase.

2. Synthesis of Ferrocenyl Acetylaniline Derivatives

The ferrocenyl acetylaniline derivatives (FcMe2Ac, FcMe3Ac and FcMe4Ac) were successfully obtained through a nucleophilic substitution strategy involving a ferrocenylmethyl quaternary ammonium intermediate and the corresponding aminoacetophenone isomers. The adopted synthetic route demonstrated high reliability and reproducibility, affording the desired products as yellow to orange crystalline solids under relatively mild experimental conditions.

The reaction pathway is depicted in Figure 7, which outlines the key mechanistic steps leading to the formation of the C–N bond at the ferrocenylmethyl position.

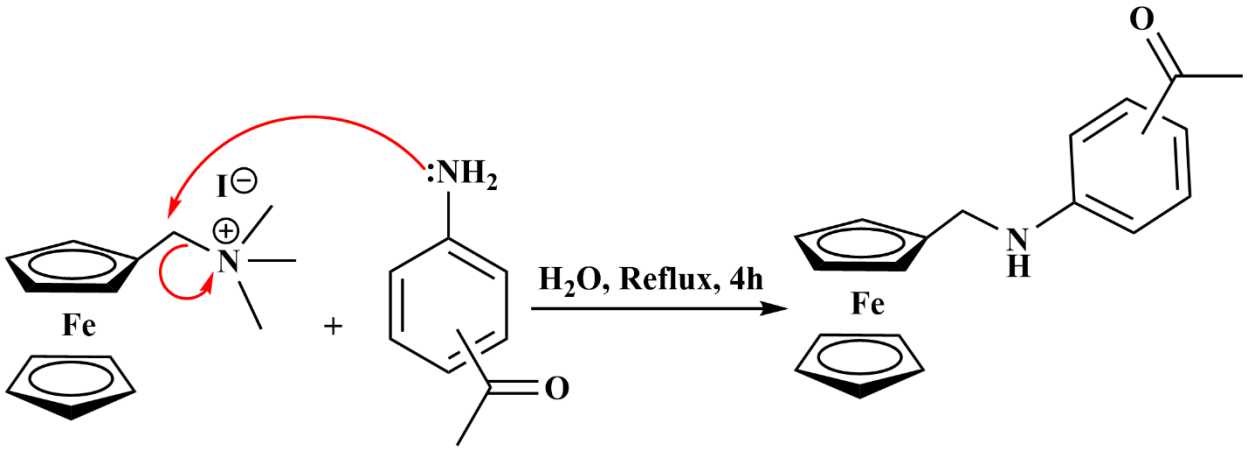

Figure 7. Proposed reaction mechanism for the formation of N-[(ferrocenyl)methyl]acetylaniline derivatives via nucleophilic substitution.

As illustrated in Figure 7, the transformation proceeds via a bimolecular nucleophilic substitution (SN2) mechanism, where the lone pair of the amino group attacks the electrophilic methylene carbon bonded to the quaternary ammonium centre. This process results in the displacement of trimethylamine as a leaving group and the formation of the ferrocenylmethylamine linkage [20].

The efficiency of this reaction can be rationalised by both electronic and structural factors. The ferrocenyl moiety exhibits electron-donating properties, which facilitate stabilisation of the transition state and enhance the reactivity of the methylene carbon [21]. In parallel, the quaternary ammonium group acts as an excellent leaving group, enabling smooth bond cleavage under aqueous conditions. Such behaviour is consistent with previously reported reactivity patterns of

ferrocenylmethyl derivatives, where favourable electronic delocalisation and structural flexibility promote nucleophilic substitution processes [22,23].

The chemical structures of the obtained compounds are presented in Figure 8, highlighting the positional variation of the acetyl substituent on the aromatic ring.

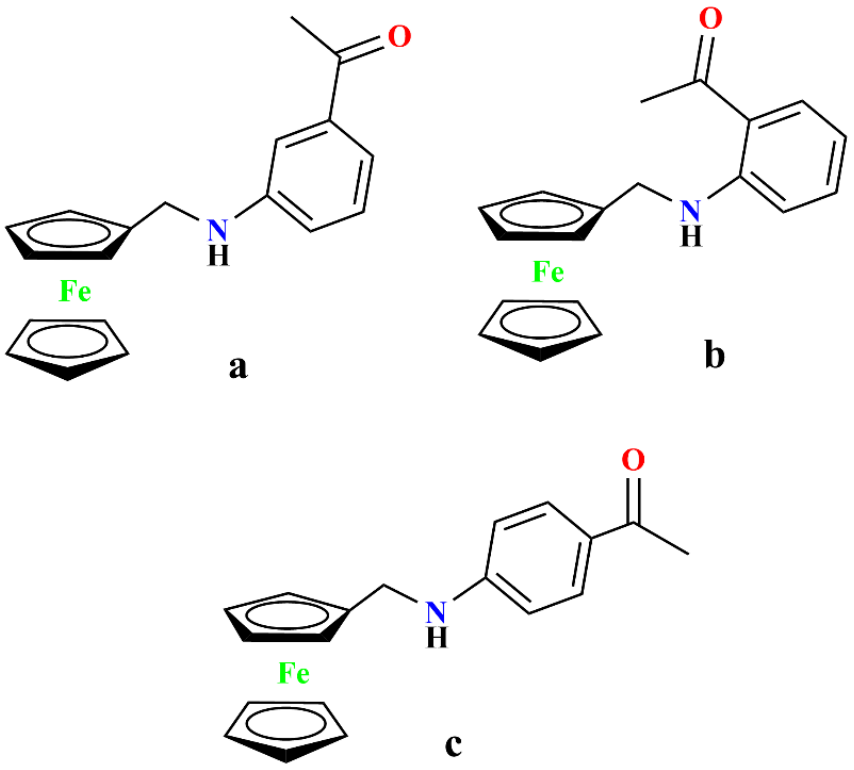

Figure 8. Chemical structures of the synthesised ferrocenyl acetylaniline derivatives: (a) FcMe2Ac (ortho), (b) FcMe3Ac (meta), and (c) FcMe4Ac (para).

As shown in Figure 8, the three derivatives differ solely by the position of the acetyl group, which significantly influences steric accessibility and electronic distribution within the molecule. These factors are known to play a critical role in modulating the nucleophilicity of the amino group and, consequently, the efficiency of the substitution reaction [24].

To further evaluate the synthetic performance, the yields and physical characteristics of the obtained compounds are summarised in Table 1.

Table 1. Yields and physical properties of the synthesised ferrocenyl acetylaniline derivatives.

Compound	Substituent Position	Yield (%)	Appearance	Melting Point (°C)

FcMe2Ac	Ortho	77	Yellow crystalline solid	148–150
FcMe3Ac	Meta	48	Yellow–orange solid	138–140
FcMe4Ac	Para	80	Deep yellow solid	162–164

As shown in **Table 1**, the reaction yields follow the order: FcMe4Ac > FcMe2Ac > FcMe3Ac

This trend can be rationalised by considering both steric and electronic effects, which are known to govern nucleophilic substitution reactions in aromatic amines. The para-substituted derivative (FcMe4Ac) exhibited the highest yield (80%), reflecting minimal steric hindrance and favourable resonance interaction between the acetyl group and the amino functionality. This electronic delocalisation enhances the nucleophilicity of the amine, thereby facilitating the substitution process [25].

In contrast, the meta derivative (FcMe3Ac) showed a significantly lower yield (48%), which can be attributed to the absence of resonance interaction between the substituents. In the meta position, the acetyl group exerts mainly an inductive electron-withdrawing effect, reducing the electron density on the amino group and consequently its nucleophilicity.

The ortho derivative (FcMe2Ac) presented intermediate behaviour (77%), where steric hindrance between adjacent substituents partially limits the accessibility of the nucleophilic site, despite favourable electronic effects.

These observations are in good agreement with previously reported studies on substituted aniline derivatives, where both steric congestion and electronic factors significantly influence reactivity. Furthermore, the results confirm that the adopted synthetic strategy is robust and well adapted for the preparation of ferrocenyl derivatives with controlled structural variation [26].

3. FT-IR Spectral Analysis

The structural features of the synthesised ferrocenyl acetylaniline derivatives were initially investigated by Fourier-transform infrared (FT-IR) spectroscopy. The recorded spectra for FcMe2Ac, FcMe3Ac and FcMe4Ac are presented in Figure 9, while the principal absorption bands and their corresponding assignments are summarised in Table 2.

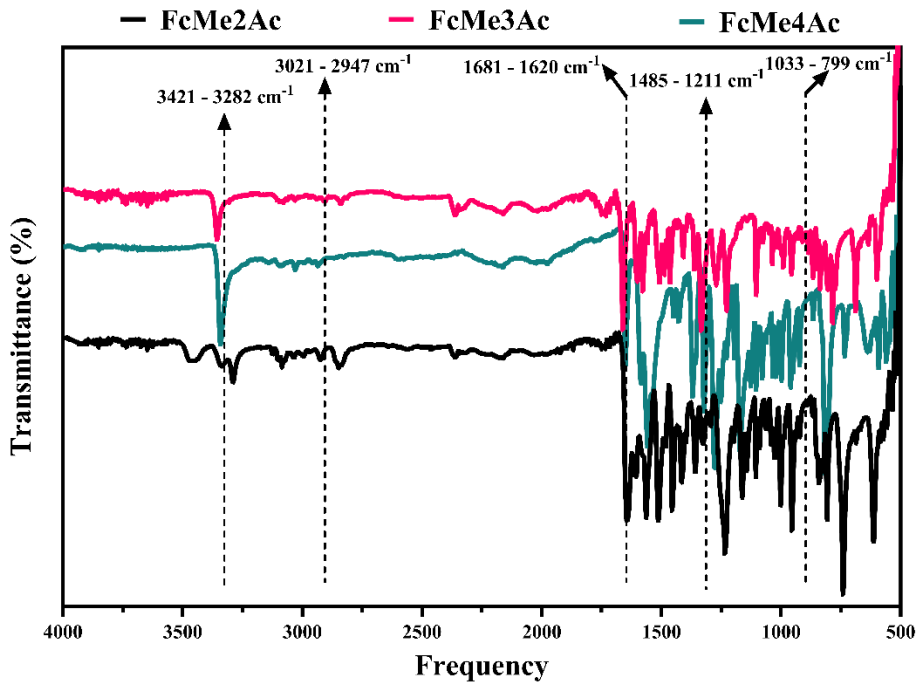

Figure 9. FT-IR spectra of the synthesised ferrocenyl acetylaniline derivatives.

Table 2. Characteristic FT-IR absorption bands (cm^{-1}) and their assignments for the synthesised compounds.

Assignment	FcMe2Ac (cm^{-1})	FcMe3Ac (cm^{-1})	FcMe4Ac (cm^{-1})	Description
N–H stretching	3426, 3291	3432, 3338	3445, 3345	Secondary amine vibration
Ar–C–H stretching	3082	—	—	Aromatic C–H
C=O stretching	1647	1650	1651	Acetyl carbonyl group
C=C (aromatic)	1566, 1516	1582, 1510	1589, 1562	Aromatic ring vibrations
C–N stretching	1146	1170	1173	Amine linkage
C–H bending	1454, 1416	1450, 1365	1369	Methyl/aromatic bending
Out-of-plane C–H	1003, 617	820	822	Aromatic substitution pattern

As shown in Figure 9, all compounds display closely related spectral profiles, confirming the preservation of the ferrocenyl acetylaniline framework across the series. Minor variations in band positions and intensities are observed and can be attributed to the different substitution patterns on the aromatic ring [27].

Broad absorption bands in the region 3445–3291 cm^{-1} are assigned to N–H stretching vibrations, confirming the presence of secondary amine functionality formed during the nucleophilic substitution reaction. The slight shifts observed between the derivatives reflect variations in hydrogen bonding interactions and local electronic environments [28].

The strong and well-defined bands located at 1651–1647 cm^{-1} correspond to the stretching vibration of the carbonyl (C=O) group of the acetyl substituent. The consistency of this band across all compounds confirms that the carbonyl functionality remains intact during synthesis.

Aromatic C=C stretching vibrations are observed in the region 1589–1510 cm^{-1}, providing clear evidence for the presence of the substituted benzene ring. Additionally, the bands detected between 1173–1146 cm^{-1} are attributed to C–N stretching vibrations, confirming the successful formation of the ferrocenylmethyl–aniline linkage.

Particularly informative are the out-of-plane C–H bending vibrations observed between 820 and 617 cm^{-1}, which are highly sensitive to substitution patterns. The differences in these bands among the ortho, meta and para derivatives provide strong evidence for the positional variation of the acetyl group on the aromatic ring.

Overall, the FT-IR data provide clear confirmation of the successful synthesis of the target compounds. The observed spectral features are fully consistent with the proposed structures and align well with reported data for related ferrocenyl and substituted aniline systems [29].

4. UV–Visible Spectral Analysis

The electronic absorption properties of the synthesised ferrocenyl acetylaniline derivatives were investigated using UV–visible spectroscopy in DMSO. The corresponding spectra are presented in Figure 10, and the absorption maxima are summarised in Table 3.

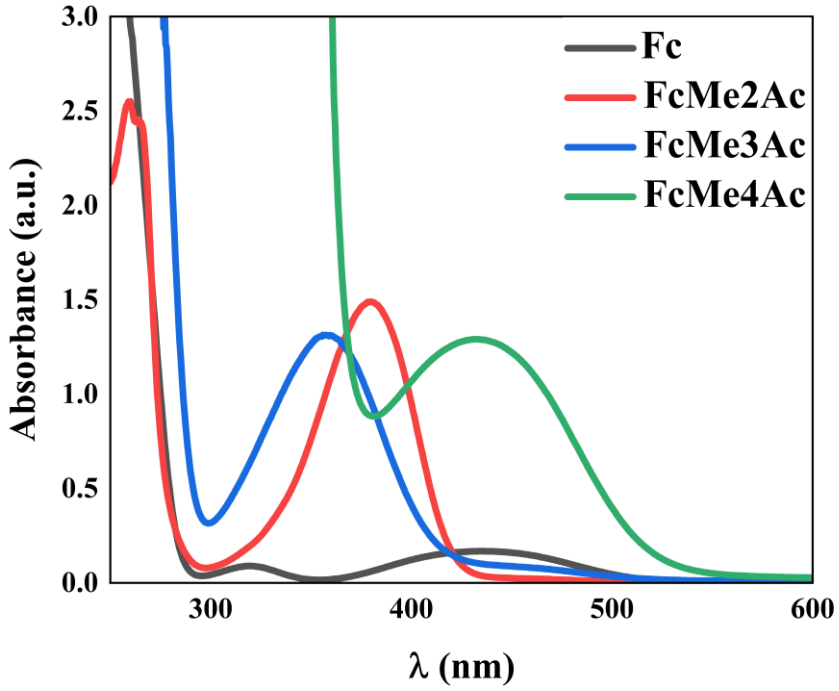

Figure 10. UV–visible absorption spectra of the synthesised ferrocenyl acetylaniline derivatives.

Table 3. UV–visible absorption maxima (λmax) of the synthesised ferrocenyl acetylaniline derivatives.

Compound	λmax (nm)	Assignment
FcMe2Ac	259	π → π* (aromatic system)
	380	d–d (Fe^{2+} centre)
FcMe3Ac	268	π → π*
	402	d–d transition
FcMe4Ac	432	d–d / charge transfer

As illustrated in Figure 10, all compounds exhibit characteristic absorption bands associated with both the aromatic system and the ferrocenyl moiety. Intense bands in the ultraviolet region (**259–268 nm**) are attributed to π → π* transitions within the conjugated aromatic system, corresponding to electronic excitation within the benzene ring [30].

In the visible region, absorption bands between **380 and 432 nm** are observed, corresponding to transitions involving the ferrocenyl iron centre. These transitions can be assigned to metal-

centred d–d transitions and, in some cases, ligand-to-metal charge transfer (LMCT), reflecting the interaction between the iron centre and the surrounding π-electron system [31].

A pronounced bathochromic shift is observed from FcMe2Ac (380 nm) to FcMe4Ac (432 nm), indicating an increase in electronic delocalisation in the para-substituted derivative. This behaviour arises from enhanced conjugation between the acetyl substituent and the aromatic system, which lowers the energy gap between molecular orbitals and facilitates lower-energy electronic transitions.

The meta derivative (FcMe3Ac) exhibits intermediate behaviour due to the absence of effective resonance interaction between substituents, limiting electron delocalisation. In contrast, the ortho derivative (FcMe2Ac), although capable of resonance interaction, may experience steric effects that slightly distort molecular planarity and reduce conjugation efficiency.

These observations highlight the significant influence of substituent position on the electronic structure of ferrocenyl derivatives. Such variations in electronic distribution are expected to play a key role in modulating molecular recognition and interaction behaviour with biological targets [32].

5. NMR Spectral Analysis

The structural elucidation of the synthesised ferrocenyl acetylaniline derivatives was comprehensively achieved using one-dimensional (^{1}H and ^{13}C) and two-dimensional (HSQC and HMBC) NMR techniques. These complementary analyses enabled precise assignment of all proton and carbon environments and provided unambiguous confirmation of the molecular structures. To facilitate interpretation, the spectra are presented individually for each compound, allowing direct correlation between spectral features and structural elements.

5.1. ^{1}H NMR Analysis

The ^{1}H NMR spectra of FcMe2Ac, FcMe3Ac and FcMe4Ac are presented in Figure 11.

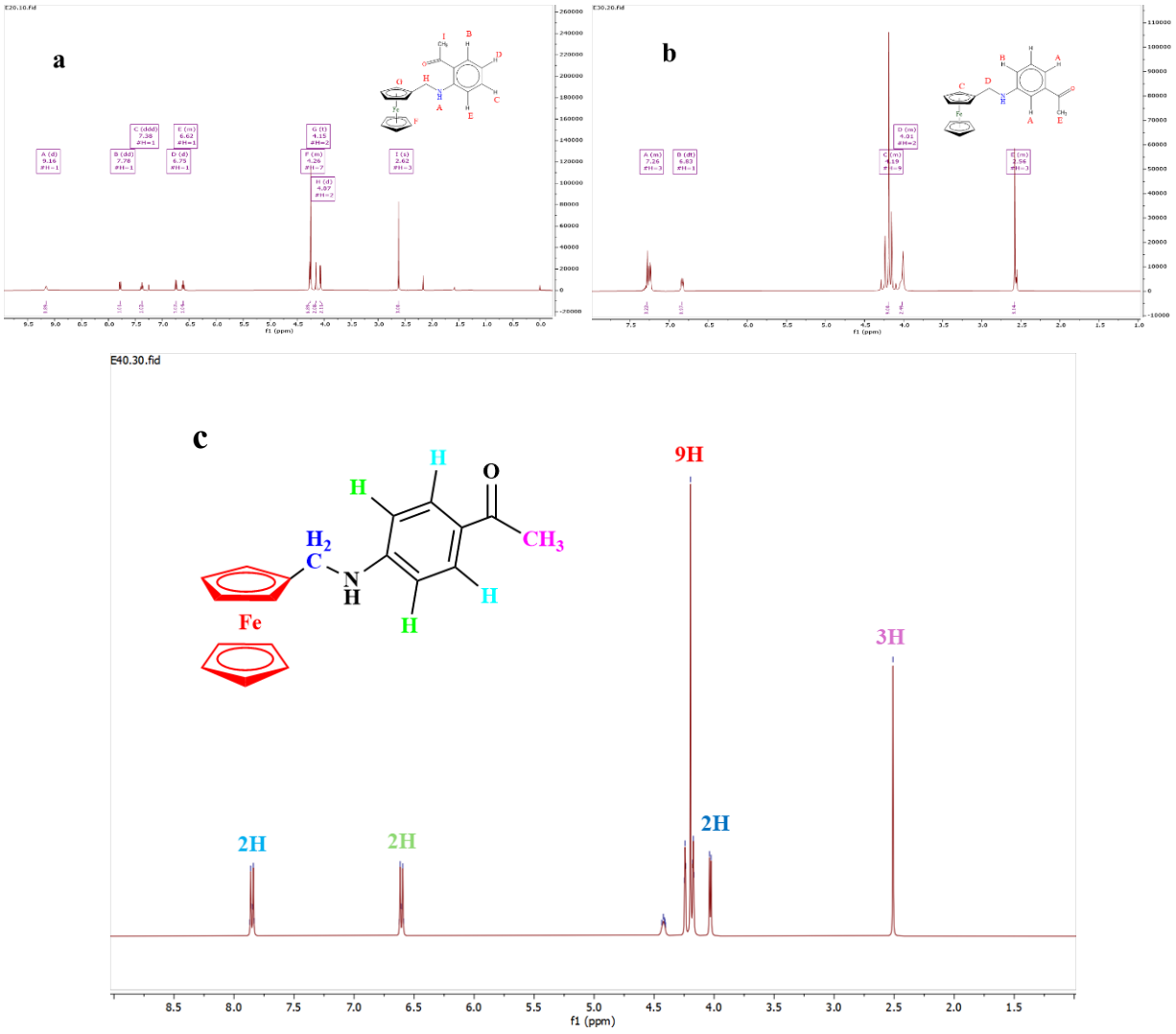

Figure 11. ^{1}H NMR spectra of the synthesised ferrocenyl acetylaniline derivatives: (a) FcMe2Ac, (b) FcMe3Ac, and (c) FcMe4Ac.

As illustrated in Figure 11, all compounds exhibit well-resolved signals consistent with the proposed molecular structures.

The methyl group of the acetyl functionality (–$COCH_3$) appears as a singlet in the region **2.35–2.60 ppm**, confirming its isolated chemical environment. The methylene bridge (–CH_2–N–), linking the ferrocenyl unit to the aromatic ring, is observed as a doublet at approximately **4.30 ppm**, providing clear evidence for the formation of the C–N bond [33].

The ferrocenyl moiety displays its characteristic spectral features. The unsubstituted cyclopentadienyl ring (C_5H_5) appears as a sharp singlet around **4.15–4.20 ppm**, reflecting its high symmetry. In contrast, the substituted cyclopentadienyl ring (C_5H_4) gives rise to multiplet signals

in the region **3.40–4.10 ppm**, indicative of reduced symmetry upon substitution. This splitting pattern is a well-established signature of monosubstituted ferrocenyl systems.

Aromatic protons are detected between **6.6 and 7.8 ppm**, exhibiting distinct splitting patterns depending on the substitution position. The ortho, meta and para isomers can be clearly differentiated based on their coupling patterns and signal multiplicity, reflecting differences in electronic distribution and proton–proton interactions within the aromatic ring.

The NH proton appears as a downfield singlet around **8.9–9.0 ppm** for FcMe2Ac and FcMe3Ac, suggesting involvement in intermolecular or intramolecular hydrogen bonding. In FcMe4Ac, a slight upfield shift is observed, which may be attributed to enhanced electronic delocalisation in the para-substituted system, reducing deshielding effects [34].

5.2. ^{13}C NMR Analysis

The ^{13}C NMR spectra of the synthesised compounds are shown in Figure 12.

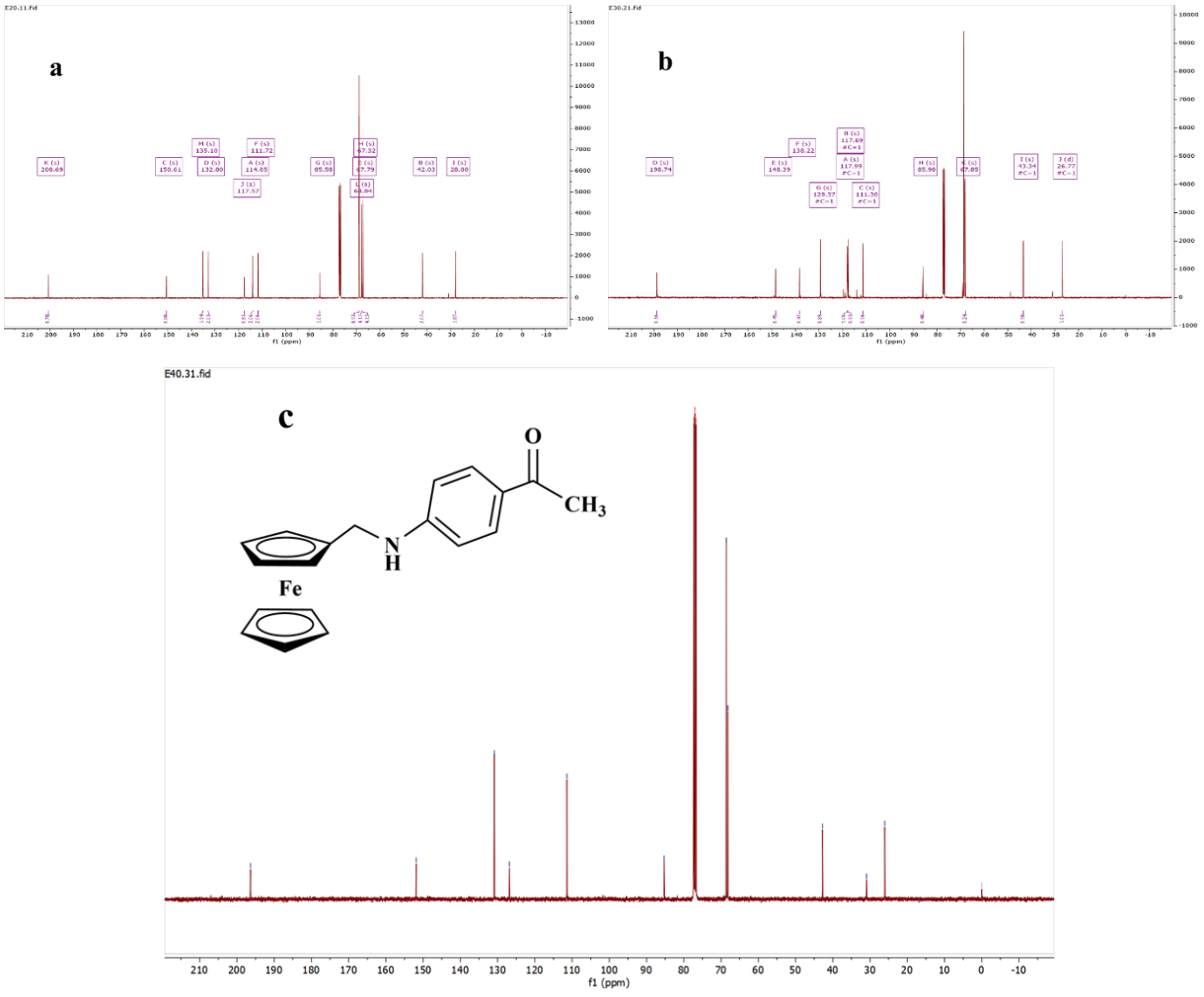

Figure 12. ^{13}C NMR spectra of the synthesised ferrocenyl acetylaniline derivatives: (a) FcMe2Ac, (b) FcMe3Ac, and (c) FcMe4Ac.

As illustrated in Figure 12, the spectra provide clear evidence for the carbon framework of the compounds.

The carbonyl carbon (C=O) is observed in the downfield region between 194 and 210 ppm, confirming the presence of the acetyl group. The variation in chemical shift among the three derivatives reflects differences in electronic environment due to substituent position.

The methylene carbon (CH_2–N) appears consistently around 42–43 ppm, confirming the linkage between the ferrocenyl moiety and the aromatic system.

The ferrocenyl carbons are detected in the range 66–69 ppm, corresponding to the cyclopentadienyl rings. The ipso carbon bonded to the substituent appears slightly downfield due to its distinct electronic environment.

Aromatic carbons are distributed between 112 and 154 ppm, with slight variations depending on substitution pattern, which is consistent with substituted benzene derivatives [35].

5.3. Two-Dimensional NMR Analysis (HSQC and HMBC)

Two-dimensional NMR spectroscopy was employed to achieve unambiguous structural assignment and to confirm the connectivity within the synthesised ferrocenyl acetylaniline derivatives. The HSQC and HMBC spectra are presented separately to allow a clear interpretation of both direct and long-range correlations.

The HSQC spectra of FcMe2Ac, FcMe3Ac and FcMe4Ac are shown in Figure 13, while the corresponding HMBC spectra are presented in Figure 14.

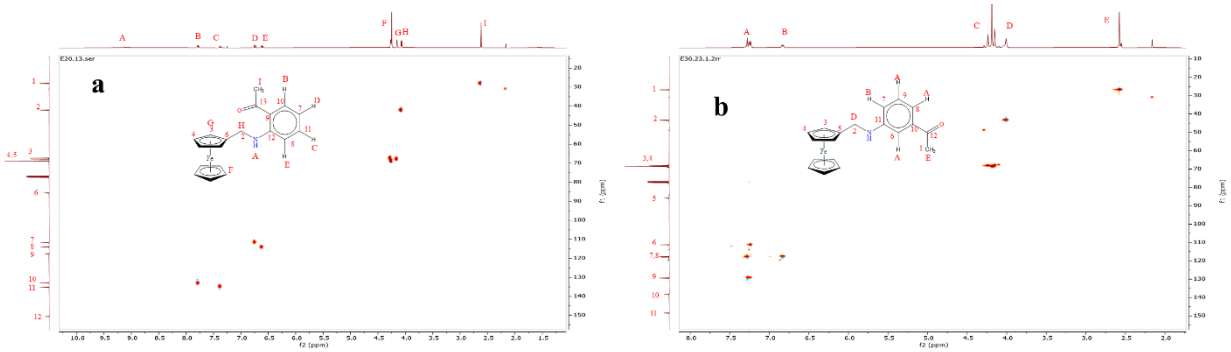

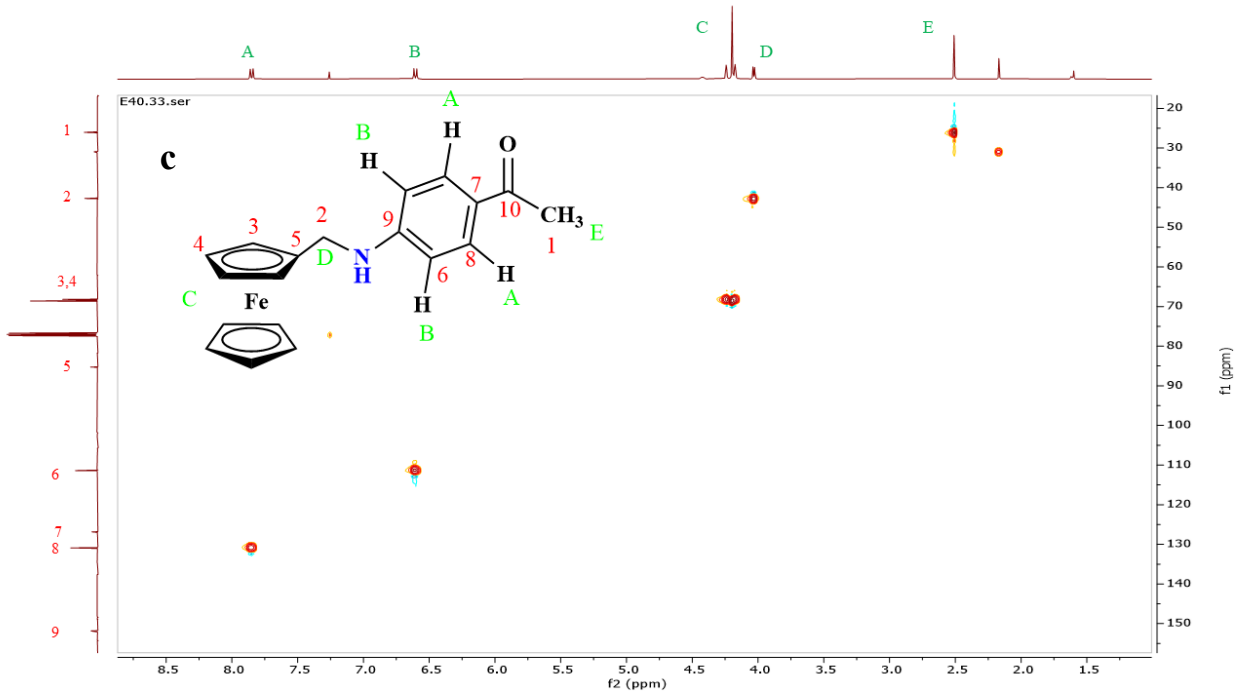

Figure 13. HSQC spectra of the synthesised ferrocenyl acetylaniline derivatives: (a) FcMe2Ac, (b) FcMe3Ac, and (c) FcMe4Ac.

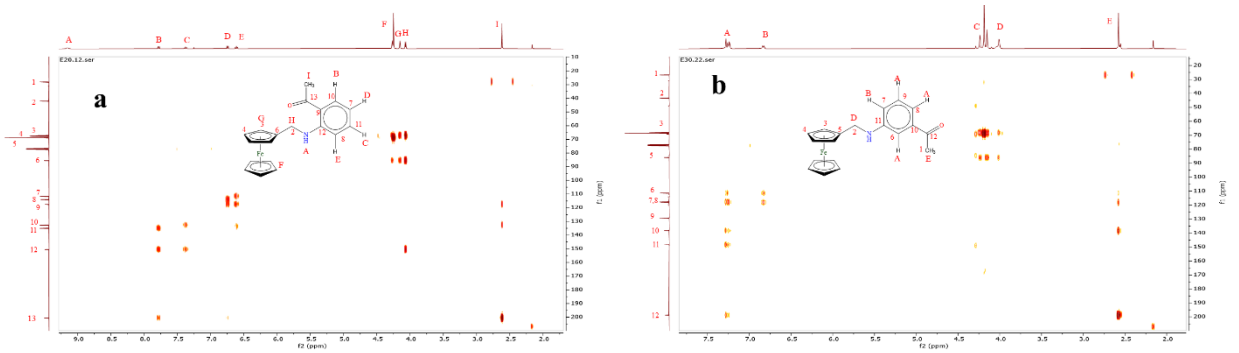

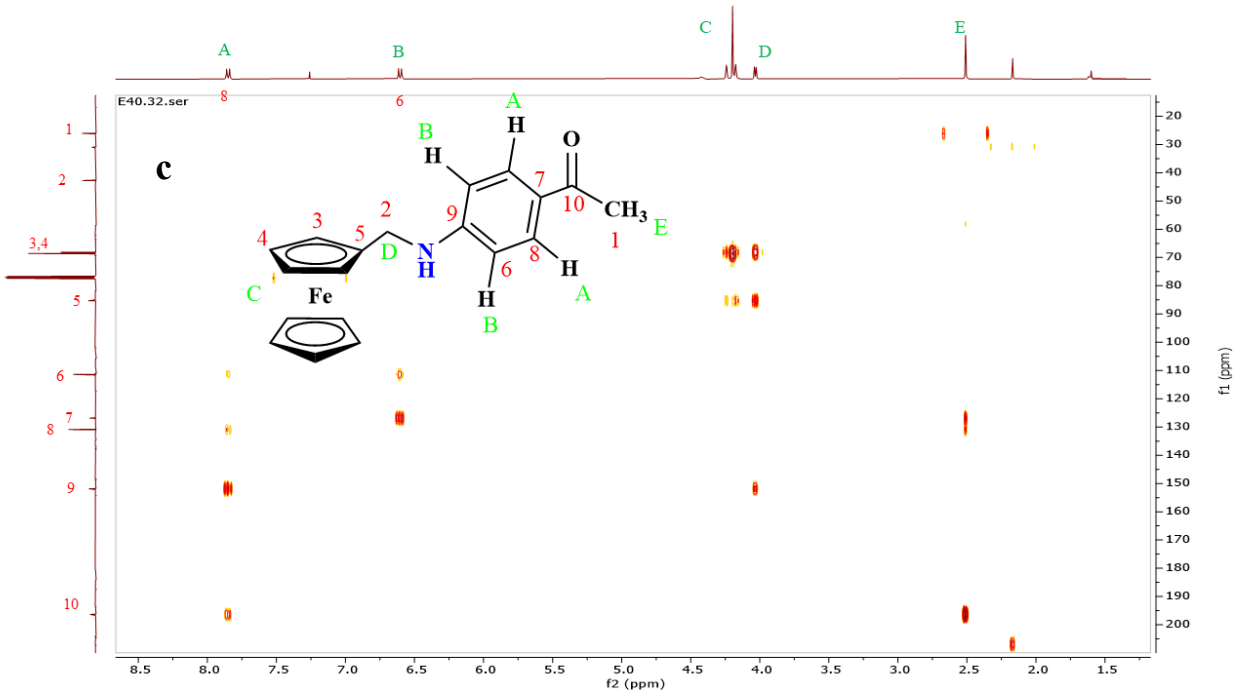

Figure 14. HMBC spectra of the synthesised ferrocenyl acetylaniline derivatives: (a) FcMe2Ac, (b) FcMe3Ac, and (c) FcMe4Ac.

As illustrated in Figure 13, the HSQC spectra provide direct one-bond correlations between proton and carbon nuclei (^{1}JCH), allowing precise assignment of all protonated carbon atoms. The methylene protons (–CH$_2$–N–), observed around 4.30 ppm in the ^{1}H NMR spectra, show clear cross-peaks with their corresponding carbon signals at approximately 42–43 ppm, confirming the presence of the ferrocenylmethyl linkage.

Similarly, the signals corresponding to the cyclopentadienyl rings exhibit well-defined correlations. The unsubstituted Cp ring (C$_5$H$_5$) shows a single correlation pattern consistent with its symmetry, whereas the substituted Cp ring (C$_5$H$_4$) displays multiple correlations reflecting the loss of equivalence upon substitution. These observations are characteristic of monosubstituted ferrocenyl systems and further confirm the structural integrity of the organometallic core.

The aromatic proton signals also show distinct HSQC correlations with their corresponding carbon atoms in the region 112–140 ppm, enabling clear assignment of the benzene ring protons. The differences observed between the ortho, meta and para derivatives further support the positional variation of the acetyl substituent [36,37].

In contrast, the HMBC spectra (Figure 14) provide long-range correlations (^{2}JCH and ^{3}JCH), which are essential for confirming the connectivity between different fragments of the molecule. In particular, strong correlations are observed between the methylene protons (–CH_2–N–) and the aromatic carbons, confirming the formation of the C–N bond linking the ferrocenyl unit to the aniline moiety.

Additional long-range correlations between aromatic protons and the carbonyl carbon (C=O) are observed, allowing precise localisation of the acetyl group on the aromatic ring. These correlations are especially important for distinguishing between the regioisomers, as the HMBC patterns differ significantly depending on the substitution position (ortho, meta or para).

Furthermore, correlations involving the ferrocenyl carbons provide additional confirmation of the substitution pattern on the cyclopentadienyl ring. The combined HSQC and HMBC data therefore establish a complete mapping of proton–carbon connectivity within the molecules [38,39].

Overall, the two-dimensional NMR analysis provides definitive structural confirmation of the synthesised ferrocenyl acetylaniline derivatives. The observed correlation patterns are fully consistent with the proposed structures and are in excellent agreement with literature reports on related ferrocenyl compounds, where HSQC and HMBC techniques are commonly used to validate substitution patterns and molecular connectivity.

6. Cyclic Voltammetry Characterization

6.1. Redox Properties and Voltammetric Response

The electrochemical properties of FcMe2Ac, FcMe3Ac and FcMe4Ac were investigated by cyclic voltammetry in DMSO (1 mM) containing 0.1 M Bu_4NBF_4 as supporting electrolyte, using Hg/Hg_2Cl_2 as reference electrode. Measurements were performed within a potential window of −0.60 to +0.60 V at a scan rate of 100 $mV \cdot s^{-1}$, with the Fc/Fc^{+} redox couple used as an internal reference.

The corresponding voltammograms are presented in Figure 15, where the responses of the substituted derivatives are compared with that of ferrocene.

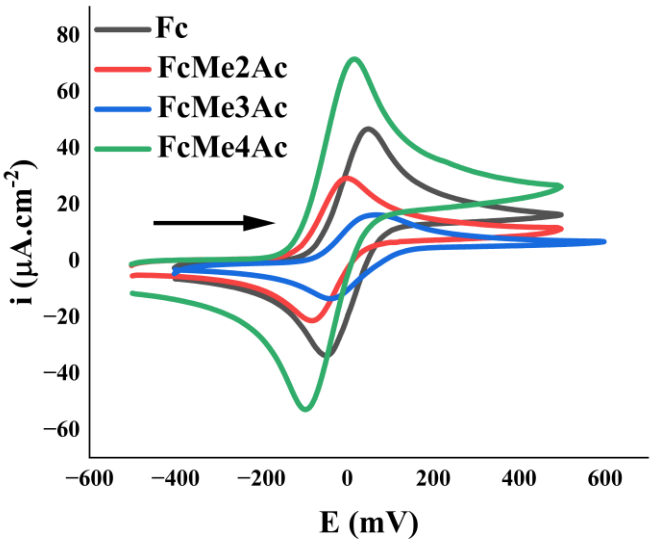

Figure 15. Cyclic voltammograms of Fc, FcMe2Ac, FcMe3Ac and FcMe4Ac recorded in DMSO containing 0.1 M Bu_4NBF_4 at a scan rate of 100 $mV \cdot s^{-1}$ (referenced to Fc^+/Fc).

As shown in Figure 15, all derivatives exhibit a single well-defined redox couple corresponding to the Fe(II)/Fe(III) transition, confirming that the ferrocenyl unit retains its electroactivity after functionalization [40].

A systematic anodic shift in formal potential is observed following the order: **FcMe2Ac (43.9 mV) < FcMe3Ac (51.0 mV) < FcMe4Ac (57.5 mV)**

This trend reflects the influence of the acetylaniline substituent on the electronic environment of the ferrocenyl centre. The positive shift indicates a decrease in electron density at the iron centre, suggesting that oxidation becomes progressively less favourable. This behaviour can be attributed to the electron-withdrawing nature of the acetyl group, which modulates the electron-donating ability of the ferrocenyl moiety through inductive and resonance effects [41].

The anodic-to-cathodic peak current ratios (Ipa/Ipc ≈ 1) indicate that the redox process is chemically reversible. However, the observed peak-to-peak separation (ΔEp = 87.8–115 mV) exceeds the theoretical value expected for an ideal reversible one-electron process (59 mV), indicating a **quasi-reversible electron transfer** [42].

This deviation suggests the presence of kinetic limitations, which may arise from:

- finite heterogeneous electron-transfer rates
- uncompensated ohmic resistance in the non-aqueous medium

- structural reorganisation accompanying oxidation of the ferrocenyl unit

6.2. Scan Rate Dependence and Mass Transport Regime

The influence of scan rate on the electrochemical response was examined in the range 100–500 mV·s⁻¹. The resulting voltammograms are shown in Figure 16, while the dependence of anodic peak current on the square root of scan rate is presented in Figure 17.

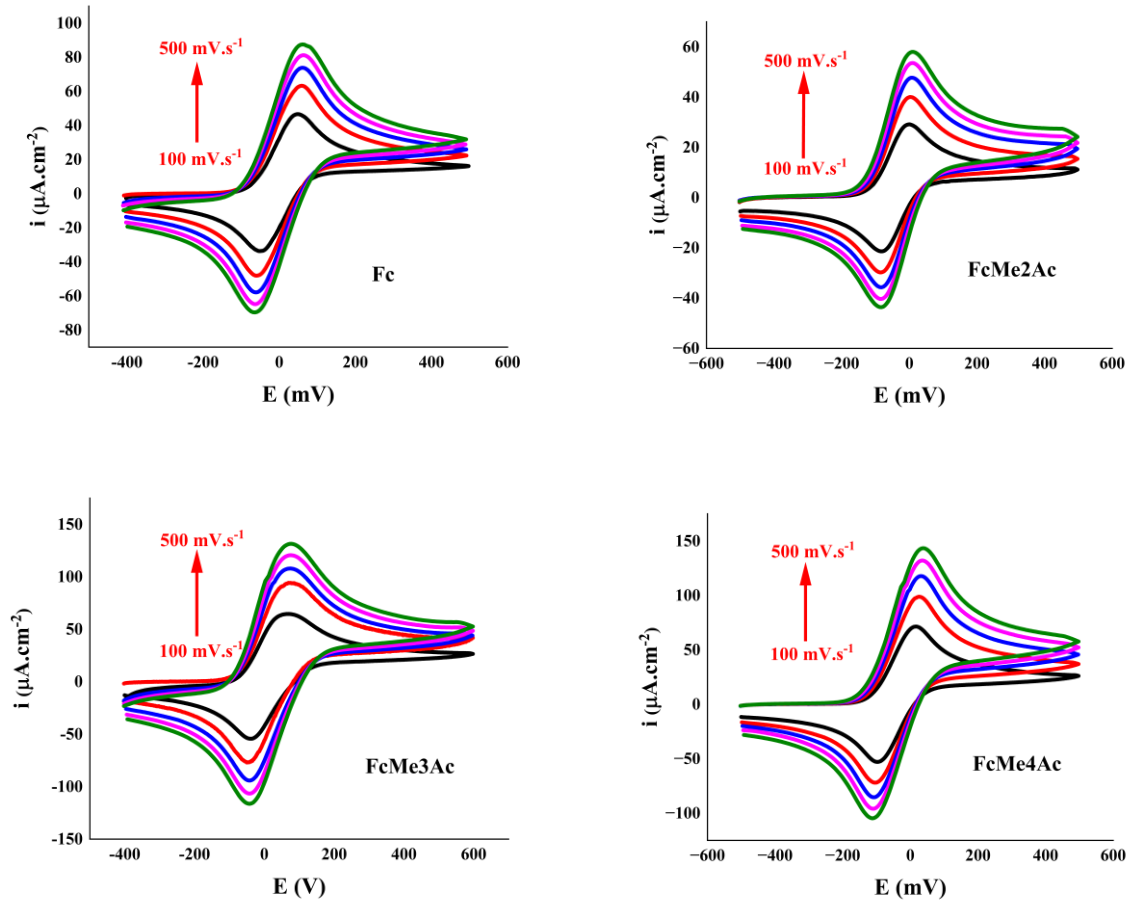

Figure 16. Cyclic voltammograms of Fc, FcMe2Ac, FcMe3Ac and FcMe4Ac at different scan rates (100–500 mV·s⁻¹).

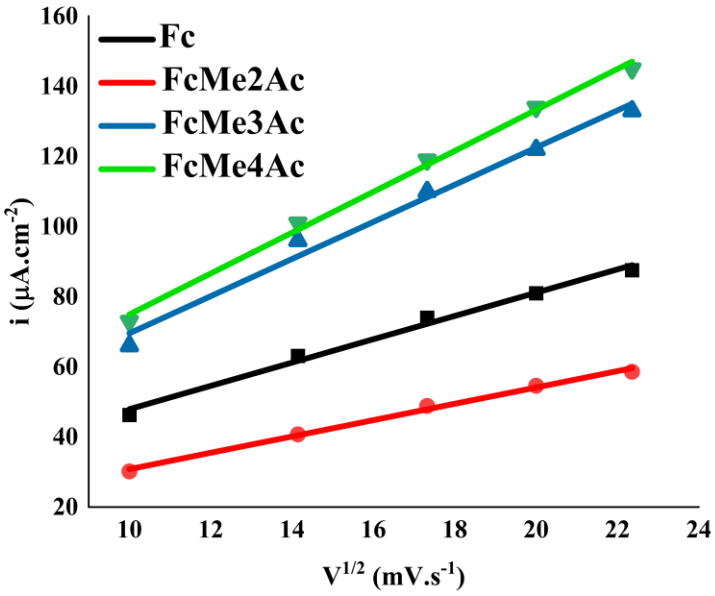

Figure 17. Linear variation of anodic peak current (i_{pa}) as a function of the square root of scan rate ($\nu^{1/2}$).

As illustrated in Figure 16, increasing the scan rate results in a proportional increase in both anodic and cathodic peak currents, without significant distortion of peak shape. This behaviour indicates that the redox process is not governed by adsorption phenomena [43].

A linear relationship between anodic peak current (i_{pa}) and $\nu^{1/2}$ is clearly observed in Figure 17 for all compounds. The corresponding linear regression equations (Table 4) exhibit high correlation coefficients (R^2 = 0.980–0.994), confirming excellent linearity [44].

The high R^2 values demonstrate that the experimental data closely follow the Randles–Ševčík model, thereby confirming that the electron transfer process is diffusion-controlled. Slight deviations from ideal linearity, particularly for FcMe3Ac (R^2 = 0.980), may reflect minor contributions from kinetic limitations or increased solution resistance [45].

6.3. Diffusion Coefficients and Transport Properties

The diffusion coefficients of the electroactive species were determined using the Randles–Ševčík Equation 1 for a reversible system, which relates the peak current to the square root of the scan rate:

$$ip_a = 2.69\times10^5\left(\sqrt{n}\right)^3 SC\sqrt{D}\sqrt{v}$$ **Equation 1**

where i_p is the peak current (A), $n$is the number of electrons transferred, A is the electrode surface area (cm^2), C is the concentration of the electroactive species ($mol.cm^{-3}$), D is the diffusion coefficient ($cm^2 \cdot s^{-1}$), and v is the scan rate ($V \cdot s^{-1}$).

The diffusion coefficients (D) were calculated using the Randles–Ševčík equation, and the results are presented in Table 4.

Table 4. Diffusion coefficients and linear regression parameters obtained from Randles–Ševčík analysis.

Compound	Equation	R^2	$D \times 10^{-7}$ ($cm^2 \cdot s^{-1}$)
Fc	y = 3.321x + 14.727	0.987	6.952
FcMe2Ac	y = 2.328x + 7.539	0.993	1.108
FcMe3Ac	y = 5.298x + 16.578	0.980	5.738
FcMe4Ac	y = 5.831x + 16.638	0.994	2.255

As shown in Table 4, the diffusion coefficients of the substituted derivatives are significantly lower than that of ferrocene. This decrease can be attributed to several physicochemical factors:

- Increased molecular volume, leading to reduced translational mobility
- Enhanced solute–solvent interactions in polar DMSO medium
- Greater structural complexity and conformational flexibility

FcMe2Ac exhibits the lowest diffusion coefficient (1.11×10^{-7} $cm^2 \cdot s^{-1}$), suggesting stronger intermolecular interactions and possibly a more hindered diffusion pathway. In contrast, FcMe3Ac retains a relatively higher diffusion coefficient, which may be associated with a more favourable molecular geometry and reduced steric constraints [46,47].

6.4. Electron Transfer Kinetics

The heterogeneous electron-transfer rate constants were estimated using Nicholson's method, which relates the peak-to-peak separation to the kinetic parameter Ψ and the standard rate constant as described in Equation 2:

$$\psi = \frac{K_s}{\sqrt{\pi D \frac{nFv}{RT}}}$$ **Equation 2**

where k_s is the standard heterogeneous electron-transfer rate constant (cm.s^{-1}), D is the diffusion coefficient (cm^2.s^{-1}), n is the number of electrons transferred, F is the Faraday constant (96,500 C.mol^{-1}), ν is the scan rate (V.s^{-1}), R is the gas constant (8.314 J.mol^{-1}.K^{-1}), and T is the absolute temperature (K).

The heterogeneous electron-transfer rate constants (k_s) were estimated using Nicholson's method, and the results are summarised in Table 5.

Table 5. Nicholson kinetic parameters (Ψ, ΔEp) and heterogeneous electron-transfer rate constants (k_s).

Compound	Ψ	ΔEp (mV)	$k_s \times 10^3$ (cm·s^{-1})
Fc	1.51	73	2.88
FcMe2Ac	0.323	124	0.62
FcMe3Ac	0.074	263	0.14
FcMe4Ac	0.100	223	0.19

The obtained kinetic parameters clearly indicate a decrease in electron-transfer rates upon substitution. The order: Fc > FcMe2Ac > FcMe4Ac > FcMe3Ac, reflects the increasing complexity of the molecular structure and its impact on electron-transfer dynamics [48].

The relatively high k_s value for ferrocene confirms its well-known fast and reversible electron-transfer behaviour. In contrast, the substituted derivatives exhibit slower kinetics, which can be explained by:

- Increased **steric hindrance**, limiting effective interaction with the electrode surface
- Higher **reorganisation energy** associated with structural changes during oxidation
- Reduced **electronic coupling** between the ferrocenyl centre and the electrode

The particularly low k_s value for FcMe3Ac suggests that the meta substitution pattern is least favourable for efficient electron transfer, likely due to suboptimal electronic communication within the molecule [49].

7. Density Functional Theory (DFT) Analysis

Density functional theory (DFT) calculations were performed to gain detailed insight into the electronic structure, reactivity and physicochemical properties of the synthesised ferrocenyl acetylaniline derivatives. These theoretical investigations provide a molecular-level interpretation

of electronic distribution and complement the experimental findings, allowing a more comprehensive understanding of structure–property relationships [50].

7.1. Frontier Molecular Orbitals and Electronic Structure

The frontier molecular orbitals (HOMO and LUMO) are key descriptors governing the reactivity of molecular systems, as they define electron-donating and electron-accepting capacities. The calculated orbital energies are summarised in Table 6, while their spatial distributions are presented in Figure 18.

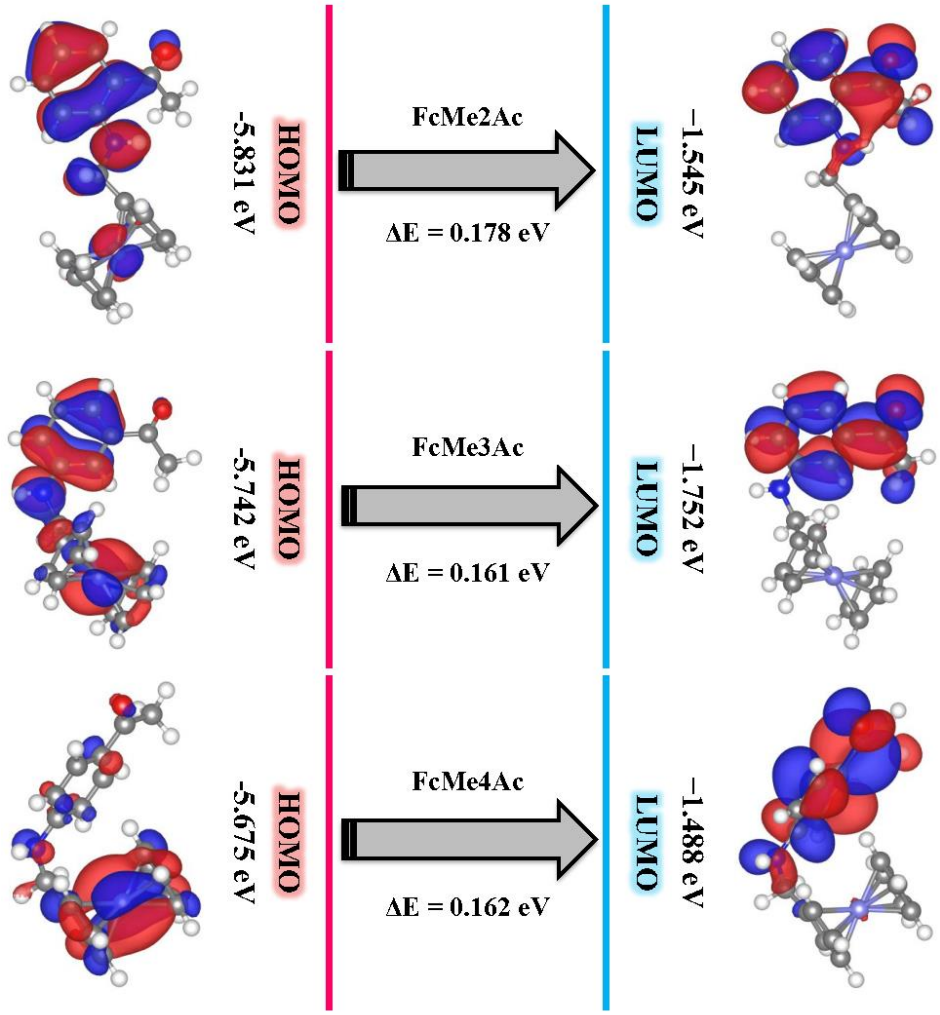

Figure 18. Frontier molecular orbitals of ferrocenyl acetylaniline derivatives: HOMO and LUMO surfaces.

Table 6. Frontier molecular orbital energies (eV) of the synthesised compounds.

Compound	EHOMO (eV)	ELUMO (eV)	ΔE (eV)
FcMe2Ac	−5.8306	−1.5453	4.285
FcMe3Ac	−5.7421	−1.7521	3.990
FcMe4Ac	−5.6752	−1.4882	4.187

The results reveal a gradual increase in HOMO energy from FcMe2Ac (−5.8306 eV) to FcMe4Ac (−5.6752 eV), indicating an enhancement of electron-donating character across the series. This trend reflects the influence of the substitution pattern on the electronic density of the ferrocenyl core, where improved conjugation promotes electron delocalisation.

The HOMO–LUMO energy gap (ΔE) ranges between **3.990 and 4.285 eV**, suggesting that all compounds possess moderate chemical stability combined with sufficient electronic flexibility. Among the derivatives, FcMe3Ac exhibits the lowest energy gap (3.990 eV), indicating increased softness and higher reactivity, whereas FcMe2Ac displays the highest gap, reflecting comparatively greater stability [51].

The orbital distribution (Figure 18) shows a clear donor–acceptor separation within the molecular framework. The HOMO is predominantly localised over the ferrocenyl moiety and partially extends towards the amine bridge, identifying this region as the principal electron donor. In contrast, the LUMO is mainly distributed over the aromatic ring and the carbonyl group, designating these sites as electron-accepting regions.

This spatial separation suggests an **intramolecular charge-transfer character**, whereby electron density is transferred from the ferrocenyl unit towards the aromatic substituent. Such donor–acceptor behaviour is particularly relevant for molecular recognition processes, as it facilitates electronic adaptation upon interaction with biological macromolecules [52].

7.2. Global Reactivity Descriptors and Thermodynamic Parameters

To further quantify molecular reactivity, global descriptors derived from frontier orbital energies were calculated and are summarised in Table 7.

Table 7. Global reactivity descriptors and thermodynamic parameters of the synthesised derivatives at 298.15 K.

Parameter	FcMe2Ac	FcMe3Ac	FcMe4Ac
Hardness, η (eV)	2.143	1.995	2.094
Electronegativity, χ (eV)	3.688	3.747	3.582

Chemical potential, μ (eV)	−3.688	−3.747	−3.582
Softness, S (eV^{-1})	0.233	0.251	0.239
Electrophilicity, ω (eV)	3.174	3.519	3.064
Nucleophilicity, N	2.829	2.918	2.985
Dipole moment (D)	3.82	4.46	5.12
Polarizability ($Å^3$)	38.5	42.7	47.3
Enthalpy ($kJ \cdot mol^{-1}$)	−1245.6	−1388.2	−1531.4
Entropy ($J \cdot mol^{-1} \cdot K^{-1}$)	412.5	448.9	486.7
Heat capacity ($J \cdot mol^{-1} \cdot K^{-1}$)	236.4	258.7	281.3

The hardness (η) values confirm that all compounds exhibit moderate stability, consistent with their HOMO–LUMO gaps. FcMe3Ac presents the lowest hardness (1.995 eV) and highest softness (0.251 eV^{-1}), reinforcing its greater electronic flexibility and reactivity.

The electrophilicity index (ω) follows the order: **FcMe3Ac > FcMe2Ac > FcMe4Ac**, indicating that FcMe3Ac has the strongest electron-accepting capability. In contrast, FcMe4Ac exhibits the highest nucleophilicity index, suggesting enhanced electron-donating potential. This duality reflects the delicate balance between donor and acceptor characteristics within the series.

The negative values of chemical potential (μ) for all compounds indicate thermodynamic stability and a natural tendency towards charge redistribution. Additionally, a progressive increase in dipole moment from FcMe2Ac to FcMe4Ac is observed, reflecting enhanced molecular polarity and asymmetry [53].

Similarly, polarizability increases across the series, indicating that the electronic cloud becomes more easily deformable. This property is particularly important for intermolecular interactions, as it enhances the ability of the molecule to adapt to external electrostatic environments.

Thermodynamic parameters, including entropy and heat capacity, also show an increasing trend, suggesting greater molecular flexibility and a higher number of accessible vibrational states. This behaviour is consistent with increasing structural complexity and conformational freedom in the substituted derivatives [54].

7.3. Molecular Electrostatic Potential (MEP) Analysis

The molecular electrostatic potential maps provide valuable insight into charge distribution and reactive sites. The calculated MEP surfaces are presented in Figure 19.

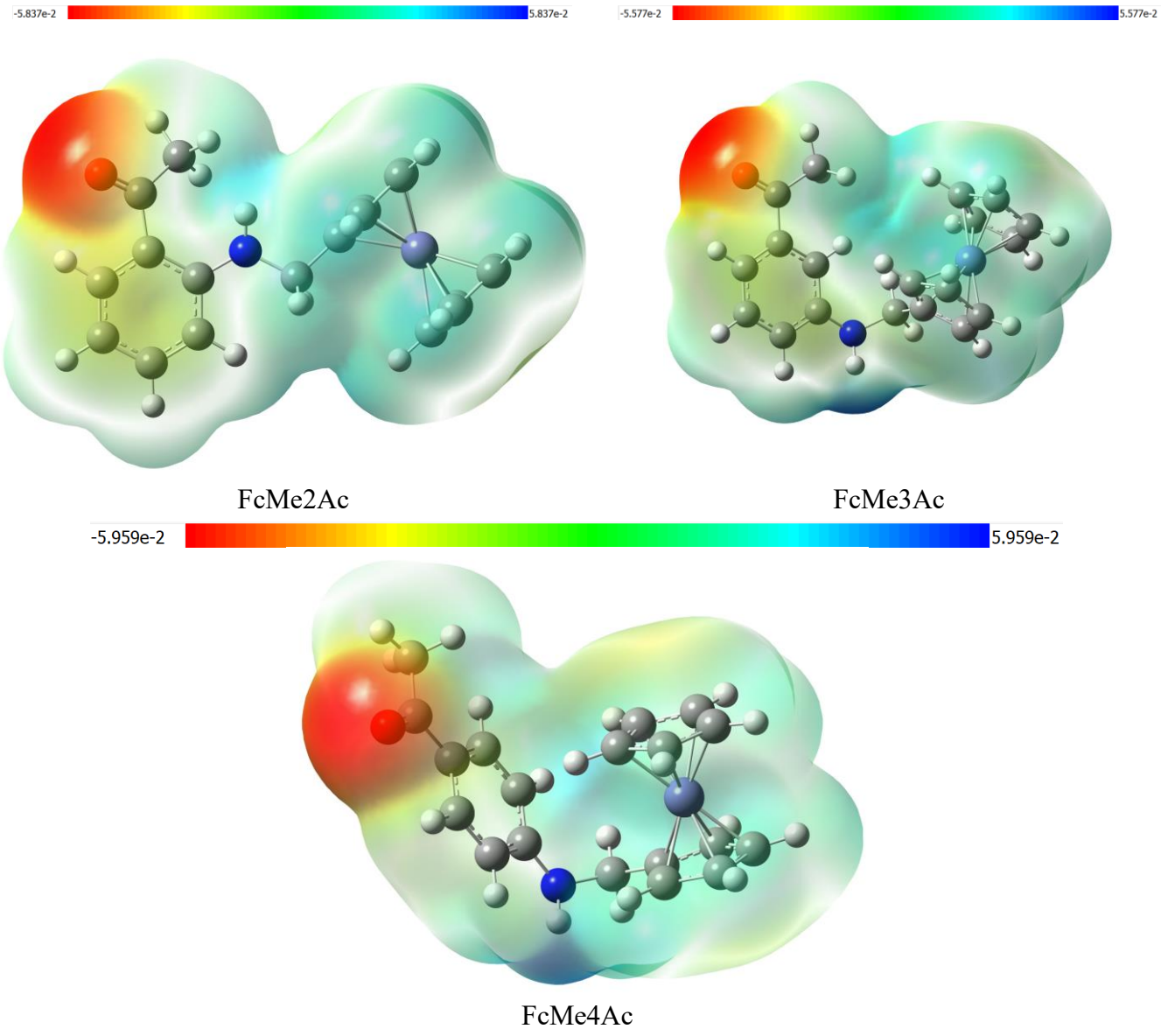

Figure 19. Molecular electrostatic potential (MEP) maps of ferrocenyl acetylaniline derivatives showing charge distribution.

The MEP analysis reveals that regions of highest negative potential are localised around the carbonyl oxygen atoms, indicating areas of high electron density and strong nucleophilic character. These regions are therefore likely to serve as preferential sites for intermolecular interactions, including hydrogen bonding and electrostatic interactions.

In contrast, positive electrostatic potential regions are primarily located around hydrogen atoms and partially over the ferrocenyl unit, corresponding to electron-deficient zones [55].

Although the overall electrostatic distribution remains similar across the three derivatives, subtle differences are observed, particularly in the para-substituted compound (FcMe4Ac), which exhibits a more delocalised charge distribution. This enhanced delocalisation may contribute to improved interaction capabilities with biological targets [56].

7.4. Electron Localisation and Non-Covalent Interaction Analysis

To further investigate electronic behaviour, ELF, LOL and RDG analyses were performed. Representative maps are presented in Figure 20 and 21.

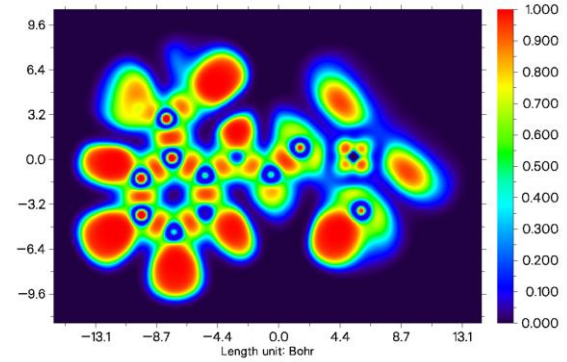

ELF_ **FcMe2Ac**

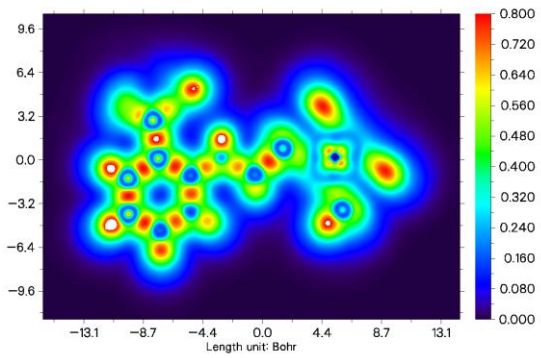

LOL_ **FcMe2Ac**

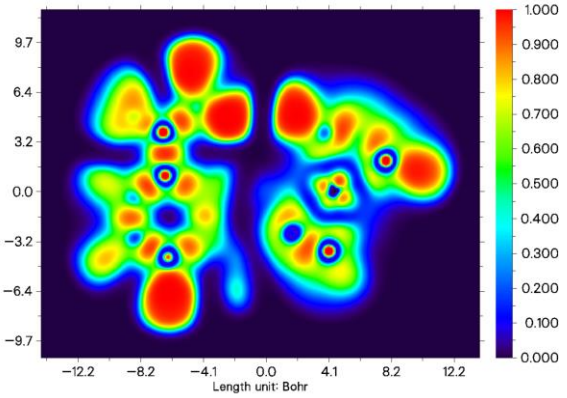

ELF_ **FcMe3Ac**

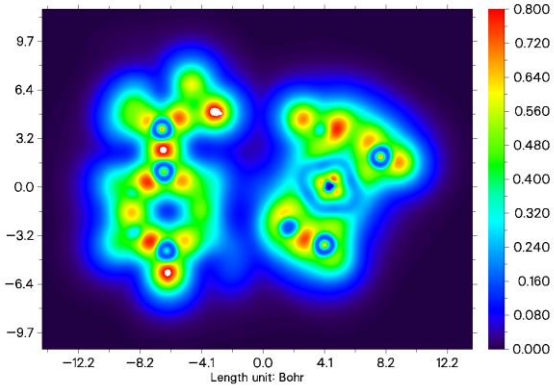

LOL_ **FcMe3Ac**

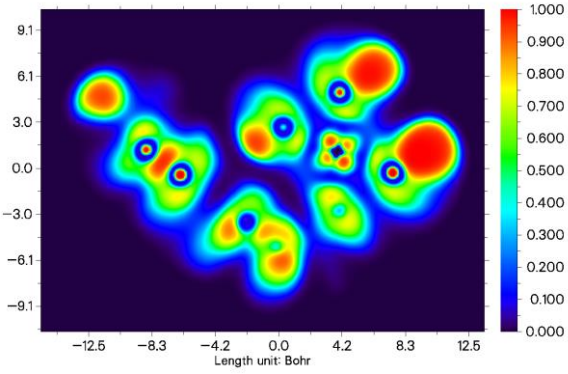

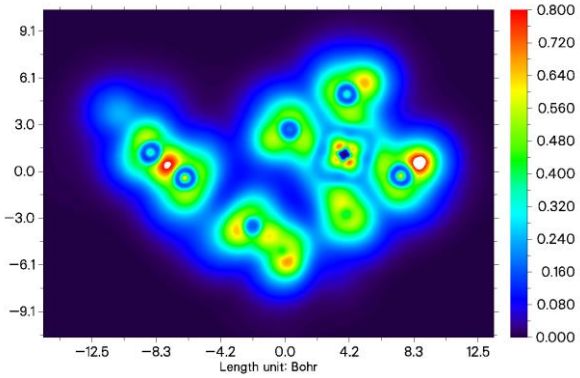

ELF_ **FcMe4Ac** LOL_ **FcMe4Ac**

Figure 20. Electron localisation (ELF and LOL) analyses of FcMeAc.

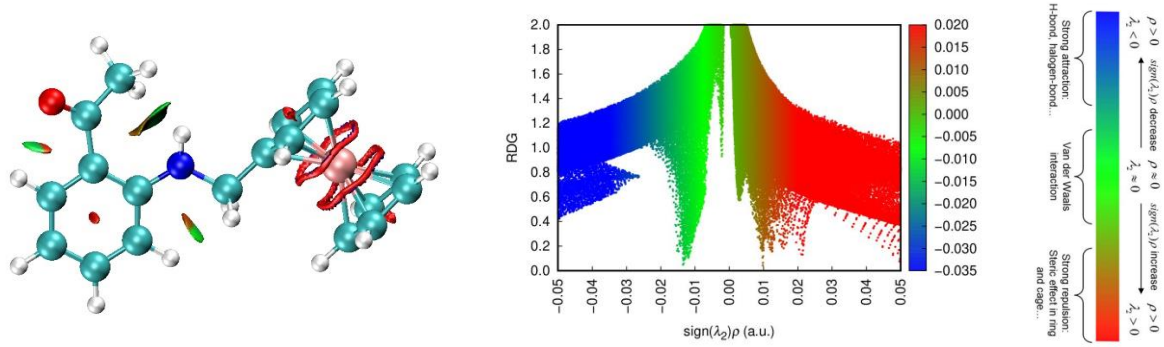

NCI_ **FcMe2Ac** RDG_ **FcMe2Ac**

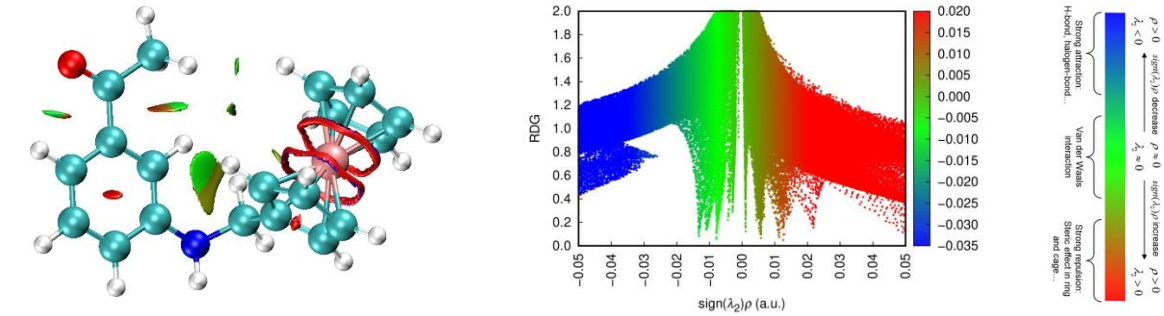

NCI_ **FcMe3Ac** RDG_ **FcMe3Ac**

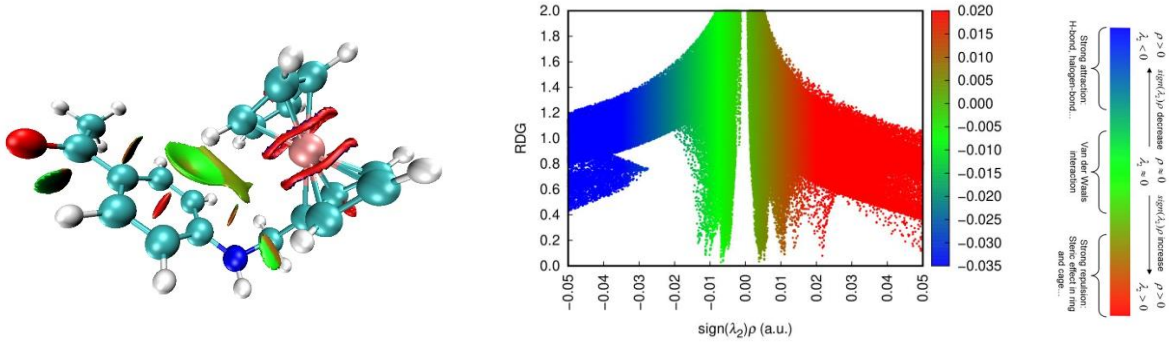

NCI_ **FcMe4Ac** RDG_ **FcMe4Ac**

Figure 21. Non-covalent interaction (RDG/NCI) analyses of FcMeAc.

The ELF and LOL maps clearly show strong electron localisation within the cyclopentadienyl rings and the aromatic system, reflecting extensive π-electron delocalisation. Localised electron density around nitrogen and oxygen atoms corresponds to lone-pair regions, which are important for intermolecular interactions.

The RDG analysis highlights weak non-covalent interactions, including van der Waals contacts and steric repulsion zones. These interactions contribute to the overall stability and conformational behaviour of the molecules.

The consistency of these features across the series indicates that the fundamental electronic structure of the ferrocenyl core is preserved, while substitution mainly modulates peripheral electronic properties [57,58].

8. Molecular Docking Study

To investigate the molecular recognition and binding behaviour of the synthesised ferrocenyl acetylaniline derivatives, molecular docking simulations were performed. The study aimed to evaluate the binding affinity, preferred orientations, and interaction patterns of the compounds within the **ATP-binding pocket of bacterial DNA gyrase (GyrB)**, a key enzymatic target involved in DNA supercoiling and replication and widely recognised in antibacterial drug development.

8.1. Docking Protocol Validation

Prior to analysing ligand–protein interactions, the reliability of the docking protocol was assessed through a **redocking procedure of the co-crystallised ligand** into the ATP-binding site of DNA gyrase (PDB ID: 6RKS). The superposition between the crystallographic and predicted binding conformations is presented in Figure 22.

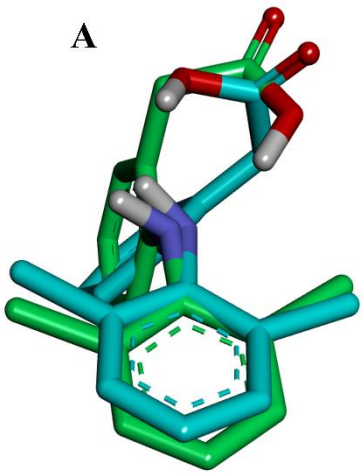

Figure 22. Superposition of the co-crystallised ligand and the redocked pose within the ATP-binding pocket of DNA gyrase (validation of docking protocol).

The calculated root-mean-square deviation (RMSD) between the experimental and redocked conformations was found to be **0.339 Å**, which is significantly lower than the commonly accepted threshold of **2.0 Å**. This result demonstrates excellent agreement between predicted and experimental ligand orientations, confirming the accuracy of the docking parameters, grid definition, and scoring function.

The very low RMSD value indicates that the adopted docking protocol is highly reliable for reproducing the native binding mode within the **ATP-binding domain of DNA gyrase**, which is critical for enzymatic activity. Consequently, this validated docking setup can be confidently applied to the ferrocenyl derivatives for subsequent interaction analysis and binding affinity evaluation.

Furthermore, the successful reproduction of the co-crystallised ligand pose confirms that the defined grid box and docking parameters appropriately capture the key structural features of the binding pocket, including residues involved in ATP recognition and inhibitor binding. This ensures that the predicted ligand–enzyme interactions are both structurally meaningful and mechanistically relevant in the context of antibacterial inhibition [59].

8.2. Binding Affinity and Energetic Analysis

The molecular docking results obtained for the ferrocenyl acetylaniline derivatives against **bacterial DNA gyrase (GyrB ATP-binding domain, PDB ID: 6RKS)** are summarised in Table 8. The calculated binding energies and energetic contributions provide detailed insight into the strength and nature of ligand–enzyme interactions within the ATP-binding pocket.

Table 8. Molecular docking results of ferrocenyl acetylaniline derivatives against DNA gyrase (GyrB ATP-binding domain).

Compound	Intermolecular Energy (kcal·mol⁻¹)	Internal Energy (kcal·mol⁻¹)	Torsional Energy (kcal·mol⁻¹)	Binding Energy (kcal·mol⁻¹)
FcMe2Ac	−7.96	−0.58	+0.74	−7.34
FcMe3Ac	−8.48	−0.71	+0.88	−7.92
FcMe4Ac	−9.42	−0.83	+0.96	−8.58
Reference ligand	—	—	—	−7.65

As shown in Table 8, all compounds exhibit **negative binding energies**, indicating that the interaction process within the DNA gyrase ATP-binding pocket is thermodynamically favourable and occurs spontaneously.

A clear affinity trend is observed: **FcMe4Ac (−8.58) > FcMe3Ac (−7.92) > FcMe2Ac (−7.34) > reference ligand (−7.65)**

This ranking demonstrates that FcMe4Ac exhibits the strongest binding affinity, surpassing the reference ligand, and therefore possesses the highest potential to inhibit DNA gyrase activity. The improved binding behaviour suggests enhanced compatibility between the ligand structure and the ATP-binding pocket, which is critical for effective antibacterial inhibition.

From an energetic perspective, the **intermolecular energy contribution dominates the binding process**, confirming that stabilisation arises primarily from non-covalent interactions, including van der Waals forces, electrostatic interactions, and hydrogen bonding. The more negative intermolecular energy values observed for FcMe4Ac indicate a stronger interaction network within the enzyme active site.

The **internal energy values remain low and negative**, indicating that ligand binding does not induce significant conformational strain. This suggests that the ferrocenyl derivatives can adopt energetically favourable conformations within the ATP-binding pocket without structural distortion. In addition, the **moderate torsional energy contributions** indicate that only limited rotational adjustments are required for optimal binding, further supporting efficient ligand accommodation.

Overall, these results demonstrate that the binding affinity of the ferrocenyl derivatives is strongly influenced by substitution pattern, which governs both electronic distribution and steric compatibility within the DNA gyrase active site [60].

8.3. Binding Mode and Interaction Analysis

The three-dimensional binding conformation of the most active compound (**FcMe4Ac**) within the ATP-binding pocket of DNA gyrase is illustrated in Figure 23.

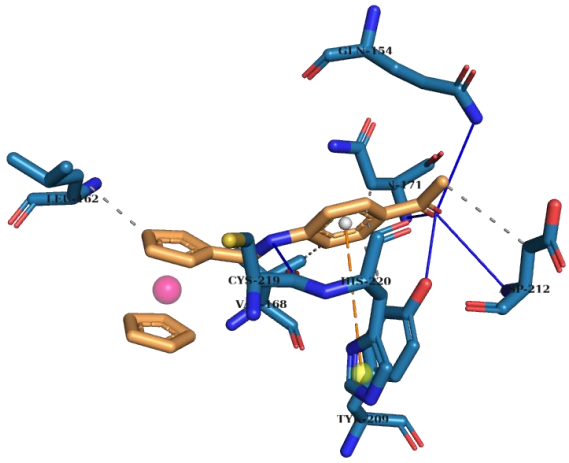

Figure 23. Three-dimensional binding mode of FcMe4Ac within the ATP-binding pocket of DNA gyrase (GyrB, PDB ID: 6RKS).

The docking results reveal that all ferrocenyl derivatives are stabilised within the **ATP-binding domain of DNA gyrase**, where the ferrocenyl core plays a central role in anchoring the ligand through hydrophobic and π-related interactions.

The interaction profile is characterised by a combination of:

- **Hydrophobic interactions** with residues such as **ILE78, VAL120, and ALA47**, contributing to ligand stabilisation within the binding pocket
- **π–π stacking interactions** between the aromatic moiety and residues such as **PHE103 and TYR5**, enhancing binding affinity
- **Hydrogen bonding interactions** involving the carbonyl group and key residues within the ATP-binding site, such as **ASP73 and GLY77**, which are essential for catalytic activity
- **Electrostatic interactions** contributing to overall stabilisation within the enzyme environment

The binding behaviour differs among the derivatives:

- **FcMe2Ac** exhibits limited interaction capacity due to steric hindrance associated with ortho substitution, resulting in fewer stabilising contacts and weaker binding affinity
- **FcMe3Ac** shows improved interaction through additional hydrogen bonding and aromatic interactions, leading to enhanced stabilisation
- **FcMe4Ac** demonstrates the most optimal binding configuration, characterised by:
    - Extensive hydrophobic contacts within the ATP-binding pocket

- Stable hydrogen bonding with key catalytic residues
- Strong π–π stacking interactions with aromatic residues
- Optimal orientation allowing efficient occupation of the ATP-binding region

This cooperative interaction network results in enhanced stabilisation of the ligand–enzyme complex and explains the superior binding affinity of FcMe4Ac compared to the other derivatives and the reference ligand [61].

8.4. Structure–Interaction Relationship

The observed differences in binding affinity and interaction behaviour can be rationalised based on structural and electronic considerations.

The **para-substituted derivative (FcMe4Ac)** exhibits the most favourable interaction profile due to its extended and symmetrical structure, which allows optimal insertion into the ATP-binding pocket of DNA gyrase. This configuration enhances steric complementarity and maximises intermolecular interactions with key residues involved in ATP recognition.

Furthermore, the higher dipole moment and increased polarizability of FcMe4Ac contribute to stronger electrostatic and dispersion interactions within the enzyme environment. Enhanced electronic delocalisation across the ferrocenyl and aromatic systems further facilitates efficient interaction with the binding site, particularly through π–π stacking and charge transfer interactions.

In contrast, the **ortho-substituted derivative (FcMe2Ac)** is affected by steric hindrance, which restricts its conformational flexibility and limits optimal accommodation within the binding pocket. This results in weaker interaction networks and reduced binding affinity.

The **meta-substituted derivative (FcMe3Ac)** exhibits intermediate behaviour, reflecting a balance between steric effects and electronic distribution. Although it forms more interactions than FcMe2Ac, its binding efficiency remains lower than that of FcMe4Ac due to less optimal spatial orientation.

Overall, these findings demonstrate that **substitution pattern plays a decisive role in modulating ligand–enzyme interactions within DNA gyrase**, directly influencing binding affinity and inhibitory potential. The results clearly identify **FcMe4Ac as the most promising candidate** for targeting bacterial DNA gyrase, highlighting its potential as a lead compound for the development of novel antibacterial agents [62].

9. Molecular Dynamics Simulation

Molecular dynamics (MD) simulations were performed to investigate the stability and dynamic behaviour of **FcMe4Ac in complex with bacterial DNA gyrase (GyrB ATP-binding domain, PDB ID: 6RKS)**. This system provides a robust structural framework for evaluating ligand binding within the ATP-binding pocket, which plays a central role in ATP hydrolysis and DNA supercoiling during bacterial replication.

9.1. System Stability: RMSD Analysis

The temporal evolution of backbone RMSD for both apo and FcMe4Ac-bound DNA gyrase systems is presented in Figure 24.

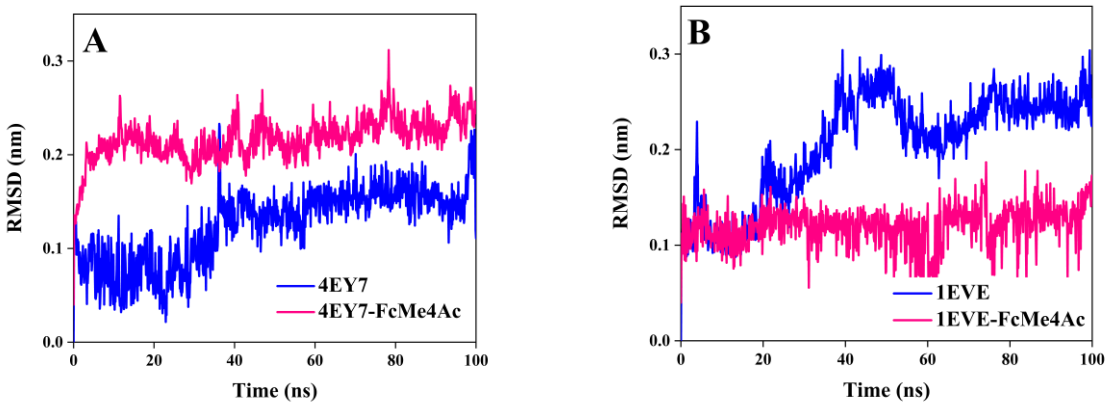

Figure 24. Figure 24. RMSD evolution of DNA gyrase (GyrB) systems: (A) apo enzyme and (B) FcMe4Ac-bound complex over 100 ns.

As shown in Figure 24, the apo DNA gyrase stabilises rapidly within approximately **0.12–0.18 nm** following the equilibration phase, indicating an intrinsically stable protein structure. Upon ligand binding, the RMSD increases moderately and stabilises within the range of **~0.18–0.26 nm**.

This slight increase reflects **ligand-induced conformational adaptation within the ATP-binding pocket**, particularly involving residues responsible for nucleotide recognition and catalytic activity. Importantly, the absence of abrupt fluctuations or long-term drift confirms that the FcMe4Ac–DNA gyrase complex remains structurally stable throughout the entire simulation time.

These results indicate that ligand binding does not destabilise the protein but instead promotes a **stable conformational state compatible with effective inhibition**, suggesting that FcMe4Ac is well accommodated within the enzyme active site [63].

9.2. Residue Flexibility: RMSF Analysis

The root-mean-square fluctuation (RMSF) profiles, presented in Figure 25, provide detailed insight into residue-level flexibility within the DNA gyrase complexes.

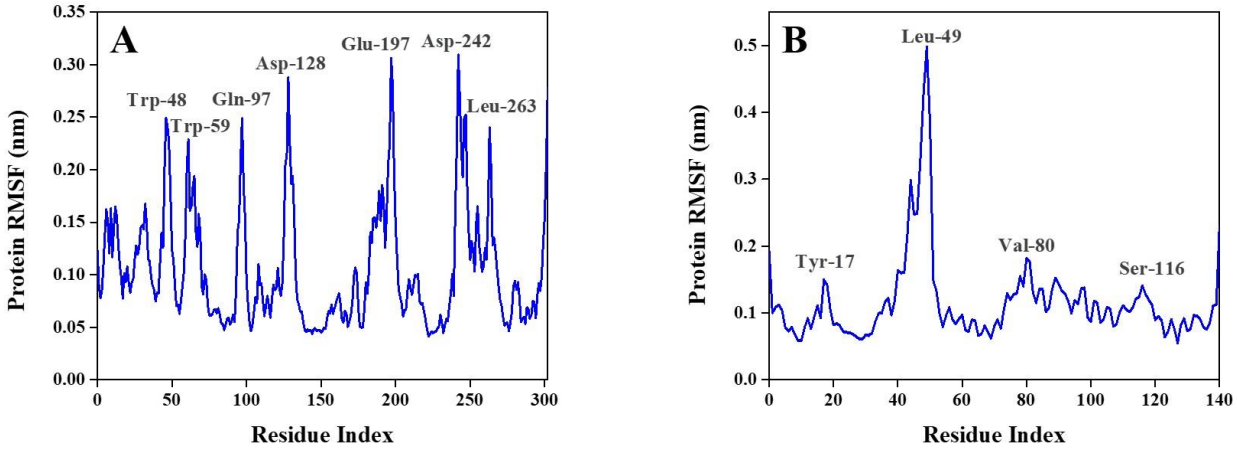

Figure 25. RMSF profiles of DNA gyrase (GyrB) residues in complex with FcMe4Ac.

The RMSF analysis reveals that the majority of residues exhibit low fluctuations (**<0.15 nm**), indicating a structurally rigid protein backbone. Increased flexibility is observed primarily in **loop regions and solvent-exposed segments**, which are inherently dynamic.

Crucially, residues located within the **ATP-binding pocket**, including **ASP73, GLY77, ILE78, VAL120, and PHE103**, display minimal fluctuations. This behaviour indicates that FcMe4Ac establishes stable interactions with key functional residues involved in ATP binding and hydrolysis.

The reduction in mobility within the active site region suggests that ligand binding induces **local rigidification**, which is often associated with effective enzyme inhibition. This stabilisation effect further supports the strong binding affinity observed in docking studies.

9.3. Ligand Stability: Ligand RMSF Analysis

The conformational stability of FcMe4Ac within the DNA gyrase binding pocket was evaluated through ligand RMSF analysis (Figure 26).

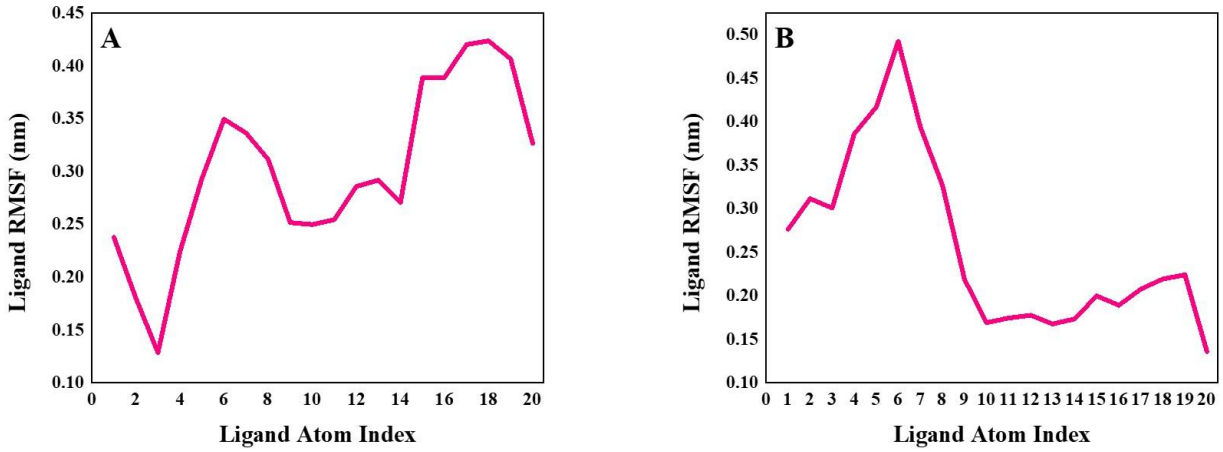

Figure 26. Ligand RMSF profile of FcMe4Ac in complex with DNA gyrase.

FcMe4Ac exhibits moderate fluctuations (**~0.12–0.22 nm**), primarily associated with peripheral substituents, while the **ferrocenyl core remains highly stable and rigid** throughout the simulation.

This observation indicates that the central organometallic scaffold is strongly anchored within the ATP-binding pocket, while peripheral functional groups retain limited flexibility, allowing adaptive interactions with surrounding residues.

The relatively low ligand RMSF values confirm that FcMe4Ac maintains a **well-defined and persistent binding conformation**, which is essential for sustained inhibitory activity.

9.4. Interaction Profile Analysis

The interaction profiles between FcMe4Ac and DNA gyrase residues during the simulation are illustrated in Figure 27.

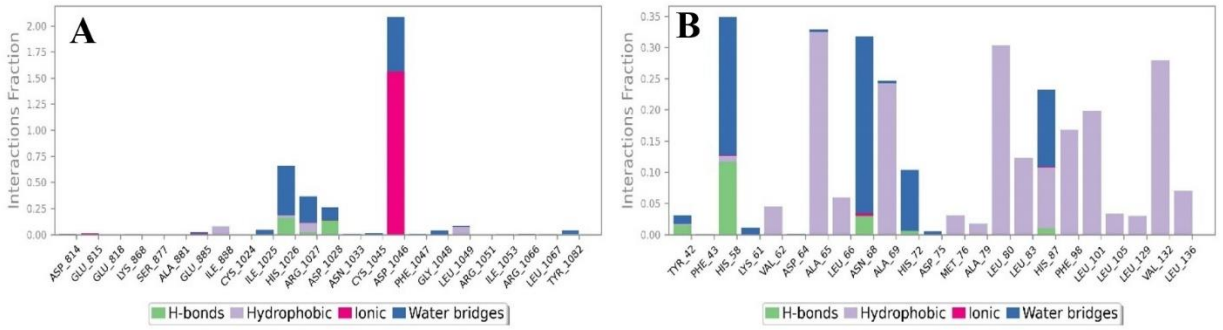

Figure 27. Interaction fraction analysis showing hydrogen bonds, hydrophobic interactions, π–π stacking, and water bridges in the DNA gyrase complex.

The stability of the complex is governed by a cooperative network of interactions, including:

- **Hydrophobic interactions** with residues such as **ILE78, VAL120, and ALA47**, contributing to ligand stabilisation within the ATP-binding pocket
- **π–π stacking interactions** with aromatic residues such as **PHE103 and TYR5**, enhancing binding affinity and electronic complementarity
- **Hydrogen bonding interactions** involving the carbonyl group of the ligand and key residues such as **ASP73 and GLY77**, which play a critical role in ATP coordination
- **Water-mediated interactions**, which contribute to the persistence and dynamic stability of the ligand–protein complex

These interactions form a **stable and synergistic network**, ensuring strong ligand retention within the ATP-binding site throughout the simulation.

Importantly, the persistence of these interactions over time highlights the ability of FcMe4Ac to effectively compete with ATP binding, thereby supporting its potential as a DNA gyrase inhibitor.

9.5. Global Structural Properties (Rg, SASA, PSA)

The evolution of global structural parameters is presented in Figure 28.

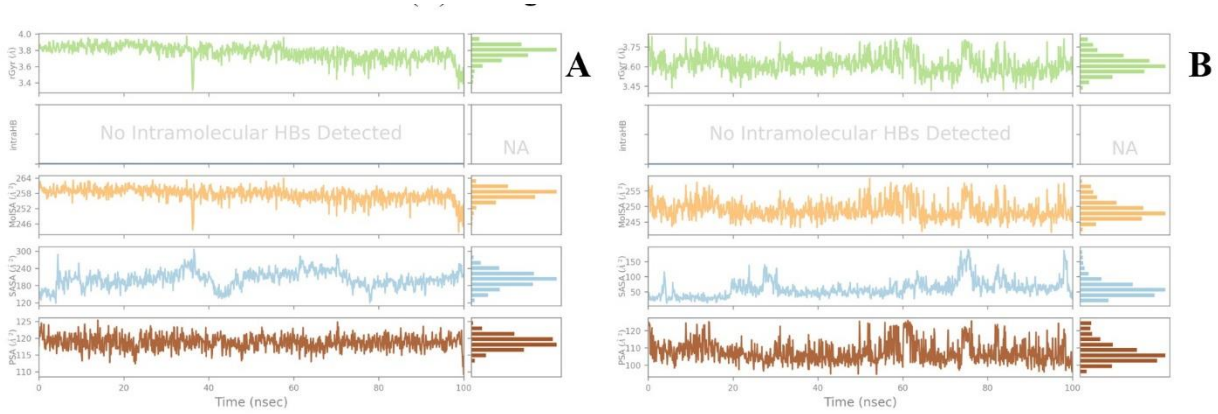

Figure 28. Time evolution of radius of gyration (Rg), molecular surface area (MolSA), solvent-accessible surface area (SASA), and polar surface area (PSA) for the DNA gyrase complex.

The radius of gyration (**Rg**) remains stable within the range of **~2.1–2.3 nm**, indicating that no significant structural unfolding or compaction occurs during the simulation.

The **SASA values** exhibit only minor fluctuations, reflecting normal solvent exposure and the absence of major conformational changes upon ligand binding. Similarly, the **polar surface area**

(PSA) remains nearly constant, suggesting that the global polarity of the enzyme is not significantly altered.

These results confirm that FcMe4Ac binding **does not disrupt the structural integrity of DNA gyrase**, but rather stabilises the protein in a conformation compatible with inhibitor binding [64].

10. ADMET Prediction and Pharmacokinetic Evaluation

To complement the structural, electronic, and dynamic investigations, the pharmacokinetic behaviour and toxicity profile of the synthesised ferrocenyl acetylaniline derivatives were evaluated using in silico ADMET prediction tools. This analysis provides essential insight into drug-likeness, absorption, distribution, metabolism, excretion, and safety characteristics, which are critical for assessing their suitability as **potential antibacterial agents targeting DNA gyrase**.

10.1. Drug-Likeness and Physicochemical Properties

The fundamental physicochemical parameters governing drug-likeness are summarised in Table 9.

Table 9. Predicted physicochemical properties and drug-likeness parameters of ferrocenyl derivatives.

Parameter	FcMe2Ac	FcMe3Ac	FcMe4Ac
Molecular weight (g·mol^{-1})	335.2	335.2	335.2
LogP (consensus)	3.12	3.28	3.45
Lipinski violations	0	0	0

All compounds comply fully with **Lipinski's rule of five**, indicating favourable characteristics for oral bioavailability. Their molecular weights (~335 g·mol^{-1}) remain well below the 500 g·mol^{-1} threshold, while LogP values (3.12–3.45) indicate **balanced lipophilicity**.

From an antibacterial drug design perspective, this level of lipophilicity is particularly advantageous, as it promotes **efficient penetration across bacterial membranes**, especially in Gram-positive strains, while maintaining sufficient aqueous solubility. The progressive increase in LogP from FcMe2Ac to FcMe4Ac reflects enhanced hydrophobic character, which may contribute to improved interaction with the largely hydrophobic ATP-binding pocket of DNA gyrase [65].

10.2. Absorption and Distribution Properties

The predicted absorption and distribution profiles are presented in Table 10.

Table 10. Predicted absorption and distribution properties of the studied compounds**.**

Parameter	FcMe2Ac	FcMe3Ac	FcMe4Ac
Gastrointestinal absorption	High	High	High
Blood–brain barrier permeability	No	No	No

All derivatives exhibit **high gastrointestinal absorption**, suggesting favourable oral bioavailability and efficient uptake upon administration.

Importantly, the predicted absence of **blood–brain barrier (BBB) permeability** is not a limitation in this context, but rather a favourable characteristic for antibacterial agents. Limited CNS penetration reduces the risk of central nervous system side effects and indicates a more **peripherally selective pharmacokinetic profile**, which is desirable for systemic antibacterial therapy.

Furthermore, the combination of high absorption and moderate lipophilicity suggests that these compounds possess **optimal permeability–solubility balance**, a key determinant of successful drug candidates [66].

10.3. Toxicological Profile

The toxicity predictions are summarised in Table 11.

Table 11. Predicted toxicity profiles of ferrocenyl acetylaniline derivatives.

Parameter	FcMe2Ac	FcMe3Ac	FcMe4Ac
Ames toxicity	No	No	No
Hepatotoxicity	No	No	No
Skin sensitisation	Low risk	Low risk	Low risk

All derivatives are predicted to be **non-mutagenic (Ames negative)** and **non-hepatotoxic**, indicating a favourable safety profile. The absence of major toxicity alerts suggests that the ferrocenyl scaffold, despite its organometallic nature, does not introduce inherent toxic liabilities in these structures.

Additionally, the **low skin sensitisation risk** supports their potential for safe handling and possible pharmaceutical development. These findings are particularly important, as toxicity remains a major limiting factor in antibacterial drug discovery [67].

10.4. Structure–Property Relationship and Comparative Analysis

The ADMET results reveal a consistent and favourable pharmacokinetic profile across the three derivatives, with clear structure–property relationships:

FcMe4Ac exhibits the highest lipophilicity, which may enhance membrane permeability and improve access to intracellular bacterial targets such as DNA gyrase

Increasing substitution on the aromatic ring contributes to **enhanced polarizability and electronic delocalisation**, which can facilitate stronger binding interactions within the ATP-binding pocket

All compounds maintain a **balanced physicochemical profile**, avoiding excessive lipophilicity that could compromise solubility or increase toxicity

Importantly, the absence of toxicity alerts, combined with compliance with drug-likeness criteria, demonstrates that structural modification of the ferrocenyl scaffold does not adversely affect safety or pharmacokinetic behaviour.

From a global perspective, these results indicate that the ferrocenyl acetylaniline derivatives possess **favourable drug-like properties compatible with antibacterial drug development**, particularly for targeting intracellular enzymes such as DNA gyrase.

Among the series, **FcMe4Ac emerges as the most promising candidate**, combining optimal lipophilicity, strong binding affinity (as demonstrated in docking and MD studies), and a favourable safety profile. This compound therefore represents a valuable lead structure for further optimisation toward the development of novel antibacterial agents [68].

CONCLUSION

General Conclusion

The present work was devoted to the rational design, synthesis, comprehensive characterisation, and advanced computational evaluation of a series of ferrocenyl acetylaniline derivatives, with particular emphasis on their potential as **inhibitors of bacterial DNA gyrase**, a key enzymatic target involved in DNA replication and a validated focus in antibacterial drug discovery. The adopted multidisciplinary strategy enabled a coherent integration of experimental and theoretical approaches, providing a robust framework for elucidating structure–property–activity relationships.

The synthetic methodology successfully yielded three regioisomeric derivatives (FcMe2Ac, FcMe3Ac, and FcMe4Ac) under mild, reproducible, and environmentally favourable conditions. Structural elucidation, achieved through FT-IR, UV–Visible spectroscopy, and one- and two-dimensional NMR techniques, unequivocally confirmed the formation of the target compounds and validated the substitution patterns on the aromatic ring. The high consistency of the spectroscopic data highlights the reliability of the synthetic route and confirms the structural integrity of the ferrocenyl scaffold.

Electrochemical investigations demonstrated that all derivatives retain the characteristic redox behaviour of the ferrocenyl core, exhibiting quasi-reversible Fe(II)/Fe(III) transitions. The observed variation in redox potentials across the series reflects the influence of acetylaniline substitution on the electronic environment of the metal centre. Furthermore, the diffusion-controlled electron-transfer processes and differences in kinetic parameters underline the sensitivity of electrochemical properties to structural modifications, which may also influence biological activity.

From a theoretical standpoint, density functional theory calculations provided detailed insight into the electronic structure and reactivity of the compounds. Frontier molecular orbital analysis revealed a pronounced donor–acceptor character, with electron density primarily localised on the ferrocenyl unit and partially delocalised over the aromatic moiety. The calculated global descriptors, supported by MEP, ELF, and RDG analyses, confirmed the presence of well-defined reactive regions and highlighted the critical role of substitution pattern in modulating electronic distribution, polarity, and interaction potential.

Molecular docking studies targeting the ATP-binding domain of DNA gyrase (GyrB) demonstrated favourable binding affinities for all derivatives. The stabilisation of ligand–enzyme

complexes was governed by a combination of hydrophobic interactions, hydrogen bonding, and π–π stacking within the ATP-binding pocket. Among the investigated compounds, FcMe4Ac consistently exhibited the strongest binding affinity, reflecting optimal steric complementarity, enhanced electronic delocalisation, and the formation of an extensive interaction network with key catalytic residues.

The stability of the ligand–protein complexes was further confirmed through molecular dynamics simulations, which revealed persistent and stable interactions under simulated physiological conditions. FcMe4Ac displayed reduced structural fluctuations, increased conformational rigidity, and a stable binding mode within the ATP-binding pocket, indicating a strong and sustained interaction with DNA gyrase.

In addition, in silico ADMET analysis demonstrated that all compounds possess favourable pharmacokinetic and safety profiles, characterised by compliance with drug-likeness criteria, high predicted gastrointestinal absorption, and absence of mutagenic or hepatotoxic risks. The lack of blood–brain barrier permeability, rather than representing a limitation, is advantageous in the context of antibacterial therapy, as it reduces the risk of central nervous system side effects and supports peripheral selectivity.

Collectively, the results demonstrate that structural modulation of ferrocenyl derivatives through acetylaniline substitution significantly influences their electronic properties, binding behaviour, and pharmacokinetic characteristics. The strong agreement between experimental findings and computational predictions further validates the reliability of the integrated methodological approach.

Among the studied compounds, **FcMe4Ac emerges as the most promising candidate**, combining optimal electronic features, strong binding affinity toward DNA gyrase, high dynamic stability, and a favourable ADMET profile. This compound represents a valuable lead scaffold for further optimisation aimed at enhancing antibacterial potency and selectivity.

In conclusion, this work provides a comprehensive and scientifically rigorous contribution to the field of **organometallic medicinal chemistry**, demonstrating the potential of ferrocenyl derivatives as versatile scaffolds for the development of novel antibacterial agents targeting DNA gyrase. The findings open promising perspectives for future experimental validation and biological evaluation, as well as for the rational design of next-generation metal-based antimicrobial compounds.

REFERENCES

BIBLIOGRAPHY

References:

[1] I.U. Khand, T. Lanez, P.L. Pauson, Ferrocene derivatives. Part 24. Synthesis of dihydro-2-pyrindines and dihydro-3 H-2-cyclopent [c] azepines by photolysis of their cyclopentadienyliron derivatives, J. Chem. Soc. Perkin 1 (1989) 2075–2078.

[2] E. Lanez, L. Bechki, T. Lanez, Antioxidant Activities, Binding Parameters, and Electrochemical Behavior of Superoxide Anion Radicals Twords 1-Ferrocenylmethylthymine and 1-Ferrocenylmethylcytosine, Curr. Phys. Chem. 10 (2020) 10–22.

[3] E. Lanez, L. Bechki, T. Lanez, Ferrocenylmethylnucleobases: Synthesis, dft calculations, electrochemical and spectroscopic characterisation, Chemistry (Easton). 14 (2020) 146–153.

[4] E. Lanez, M. Saidi, T. Lanez, Assessment of antioxidant and DPPH free radical scavenging activity of 1,2-dithiole-3-thione derivatives by using cyclic voltammetry, spectroscopic, and molecular docking studies, Journal of Sulfur Chemistry 44 (2023) 542–558. https://doi.org/10.1080/17415993.2023.2200142.

[5] H. Benamara, T. Lanez, E. Lanez, Bsa-binding studies of 2-and 4-ferrocenylbenzonitrile: Voltammetric, spectroscopic and molecular docking investigations, Journal of Electrochemical Science and Engineering 10 (2020) 335–346. https://doi.org/10.5599/jese.861.

[6] E. Lanez, L. Bechki, T. Lanez, Antioxidant Activities, Binding Parameters, and Electrochemical Behavior of Superoxide Anion Radicals Twords 1-Ferrocenylmethylthymine and 1-Ferrocenylmethylcytosine, Curr. Phys. Chem. 10 (2019) 10–22. https://doi.org/10.2174/1877946809666190424143752.

[7] E. Lanez, L. Bechki, T. Lanez, Ferrocenylmethylnucleobases: Synthesis, dft calculations, electrochemical and spectroscopic characterisation, Chemistry and Chemical Technology 14 (2020) 146–153. https://doi.org/10.23939/chcht14.02.146.

[8] E. Lanez, L. Bechki, T. Lanez, N6, 9-bis (ferrocenylmethyl) adenine: synthesis, cyclic voltammetric, spectroscopic characterization, and DFT calculations, Scientific Study & Research. Chemistry & Chemical Engineering, Biotechnology, Food Industry 20 (2019) 509–519.

[9] M.J. Frisch, G.W. Trucks, H.B. Schlegel, G.E. Scuseria, M.A. Robb, J.R. Cheeseman, G. Scalmani, V. Barone, B. Mennucci, G.A. Petersson, Gaussian 09. Wallingford, CT: Gaussian, 2009.

[10] M.P. Andersson, P. Uvdal, New scale factors for harmonic vibrational frequencies using the B3LYP density functional method with the triple-ζ basis set 6-311+ G (d, p), J. Phys. Chem. A 109 (2005) 2937–2941.

[11] T. Lu, F. Chen, Multiwfn: A multifunctional wavefunction analyzer, J. Comput. Chem. 33 (2012) 580–592.

[12] P.W. Rose, A. Prlić, A. Altunkaya, C. Bi, A.R. Bradley, C.H. Christie, L. Di Costanzo, J.M. Duarte, S. Dutta, Z. Feng, R.K. Green, D.S. Goodsell, B. Hudson, T. Kalro, R. Lowe, E. Peisach, C. Randle, A.S. Rose, C. Shao, Y.P. Tao, Y. Valasatava, M. Voigt, J.D. Westbrook, J. Woo, H. Yang, J.Y. Young, C. Zardecki, H.M. Berman, S.K. Burley, The RCSB protein data bank: Integrative view of protein, gene and 3D structural information, Nucleic Acids Res. 45 (2017) D271–D281.

[13] C. Steffen, K. Thomas, U. Huniar, A. Hellweg, O. Rubner, A. Schroer, AutoDock4 and AutoDockTools4: Automated Docking with Selective Receptor Flexibility, J. Comput. Chem. 31 (2010) 2967–2970.

[14] T. Lanez, M. Lanez, R. Lanez, E. Lanez, B. Talbi-Lanez, Computational Screening of Novel Nitroimidazole Candidates: Targeting Key Enzymes of Oral Anaerobes for Anti-Parasitic Potential, Curr. Drug Discov. Technol. (2024).

[15] E. Lanez, N. Zegheb, T. Lanez, In silico ADME, toxicological analysis, molecular docking studies and Molecular dynamics simulation of Afzelin with potential antibacterial effects against Staphylococcus aureus, Turkish Computational and Theoretical Chemistry 7 (2023) 10–16. https://doi.org/10.33435/TCANDTC.1196422.

[16] J. Huang, A.D. Mackerell, CHARMM36 all-atom additive protein force field: Validation based on comparison to NMR data, J. Comput. Chem. 34 (2013) 2135–2145. https://doi.org/10.1002/jcc.23354.

[17] K. Vanommeslaeghe, A.D. MacKerell, Automation of the CHARMM general force field (CGenFF) I: Bond perception and atom typing, J. Chem. Inf. Model. 52 (2012) 3144–3154. https://doi.org/10.1021/ci300363c.

[18] R. Kumari, R. Kumar, A. Lynn, G-mmpbsa -A GROMACS tool for high-throughput MM-PBSA calculations, J. Chem. Inf. Model. 54 (2014) 1951–1962. https://doi.org/10.1021/ci500020m.

[19] J. Dong, N.N. Wang, Z.J. Yao, L. Zhang, Y. Cheng, D. Ouyang, A.P. Lu, D.S. Cao, Admetlab: A platform for systematic ADMET evaluation based on a comprehensively collected ADMET database, J. Cheminform. 10 (2018) 1–11. https://doi.org/10.1186/s13321-018-0283-x.

[20] P. Banerjee, A.O. Eckert, A.K. Schrey, R. Preissner, ProTox-II: A webserver for the prediction of toxicity of chemicals, Nucleic Acids Res. 46 (2018) W257–W263. https://doi.org/10.1093/nar/gky318.

[21] Y. Ouennoughi, H.E. Karce, D. Aggoun, T. Lanez, R. Ruiz-Rosas, B. Bouzerafa, A. Ourari, E. Morallon, A novel ferrocenic copper (II) complex Salen-like, derived from 5-chloromethyl-2-hydroxyacetophenone and N-ferrocenmethylaniline: Design, spectral approach and solvent effect towards electrochemical behavior of Fc+/Fc redox couple, J. Organomet. Chem. 848 (2017) 344–351.

[22] M. Chebbah, E. Lanez, S. Bouacida, H. Athmani, M.L. Ben Amor, R. Hafidi, A. Bouchemma, Synthesis, Characterization, Structural Analysis, Hirshfeld Surface Studies, and Molecular Docking of 1, 3, 5-Tris (P-Bromophenyl)-1, 3, 5-Triazacyclohexane, Hirshfeld Surface Studies, and Molecular Docking Of 1 (n.d.).

[23] M. Hanane, T. Lanez, I. Zafar, M.S. Afghan, N. Zegheb, N'-Ferrocenylmethyl-N'-phenylbenzohydrazide as a potential DNA binding compound: a combined experimental and computational study, J. Coord. Chem. 76 (2023) 1984–1998. https://doi.org/10.1080/00958972.2023.2275247.

[24] A. Adaika, Y. Bekkar, S. Youmbai, L. Bourougaa, E. Lanez, M.L. Ben Amor, K. Nesba, T. Lanez, L. Bechki, Synthesis, Antioxidant, and Antidiabetic Potential of Ferrocenylmethylnucleobase Compounds: In Vitro, In Silico Molecular Docking, DFT Calculation, and Molecular Dynamic Simulations, Appl. Organomet. Chem. 39 (2025) e7988.

[25] E. LANEZ, D. BENKHELIFA, F.Z. CHERIET, K. GORI, C. SLIMANI, S. KEBACHE, R. OUAKOUAK, O. ABDELLAOUI, Y. DJOUGHI, M.L. BENAMOR, Theoretical Investigation of Mitomycin Derivatives as Dual Inhibitors of HER2 and ER-α: Prospects

for Novel Breast Cancer Treatment Strategies, Algerian Journal of Biosciences 6 (2025) 1–20.

[26] E. Lanez, Y. Bekkar, L. Bourougaa, M.L. Benamor, R. Bouraoui, O. Boudebia, A. Adaika, K. Nesba, H. Chaoua, L. Bechki, Antidiabetic potential of mentha piperita essential oil: GC-MS profiling, in vitro, in vivo and in silico analyses, J. Mol. Struct. (2025) 144239.

[27] C. Benine, D.A. Boutlelis, L.A. Touhami, E. Lanez, D.G. Amara, G. Rim, N. Hanen, W. Zahnit, M. Messaoudi, Green synthesis, characterization, antioxidant, interaction with DNA/BSA, and investigation of cytotoxicity against MCF-7 cancer cells of zinc oxide nanoparticles using Hammada scoparia (Pomel) Iljin extract, Int. J. Biol. Macromol. 295 (2025) 139709.

[28] M.L. Tlili, I. Laib, K. Salemi, I. Chetehouna, I. BenMoussa, E. Lanez, Phytochemical Analysis and Evaluation of the Antioxidant, Anti-Inflammatory, Hemolytic, and Antibacterial Effects of Astragalus gombo (L.) Leaves., Acta Chim. Slov. 71 (2024).

[29] M.L. Tlili, F. Alia, E. Bahri, T. Beyat, K. Redouan, E. Lanez, In vivo evaluations of the antidiabetic and antioxidant effects of Olea europaea L.(Chemlali variety) leaves, Acta Periodica Technologica (2025) 3.

[30] S. Khamouli, S. Belaidi, M. Ouassaf, T. Lanez, S. Belaaouad, S. Chtita, Multi-combined 3D-QSAR, docking molecular and ADMET prediction of 5-azaindazole derivatives as LRRK2 tyrosine kinase inhibitors, J. Biomol. Struct. Dyn. 40 (2022) 1285–1298.

[31] N. Zouaghi, E. Lanez, M.L. Benamor, S.N. Nacer, T. Lanez, Y. Bekkar, H. Haddad, K. Al-Abdallat, M. Zihlif, Y. Al-Abdallat, Targeting Alzheimer's Disease via Phytochemicals from Artemisia campestris L.: GC/MS Analysis with an Integrated Computational Approach, Food Biosci. (2025) 108128.

[32] N. Zegheb, C. Boubekri, T. Lanez, E. Lanez, T.T. Küçükkılınç, E. Öz, A. Khennoufa, S. Khamouli, S. Belaidi, In Vitro and In Silico Determination of Some N-ferrocenylmethylaniline Derivatives as Anti-Proliferative Agents Against MCF-7 Human Breast Cancer Cell Lines, Anticancer Agents Med. Chem. 22 (2021) 1426–1437. https://doi.org/10.2174/1871520621666210624141712.

[33] M.L.B.E.N. AMOR, E. LANEZ, Y. Bekkar, A. ADAIKA, T. LANEZ, K. NESBA, L. BECHKI, Exploring the Interactions of Ferrocenylmethylnucleobase Derivatives With BSA

and HHb: Insights From Electrochemical, Spectroscopic, ADMET, in Silico Docking, and MD Simulations, ChemistrySelect 10 (2025) e202404678.

[34] A. Rebiai, T. Lanez, M.L. Belfar, Total polyphenol contents, radical scavenging and cyclic voltammetry of algerian propolis, Int. J. Pharm. Pharm. Sci. 6 (2014) 395–400.

[35] M.L. Ben Amor, E. Lanez, Y. Bekkar, A. Adaika, T. Lanez, K. Nesba, L. Bechki, EVALUATION OF FERROCENYLMETHYLNUCLEOBASES DERIVATIVES INTERACTING WITH DNA: INSIGHTS FROM ELECTROCHEMICAL, SPECTROSCOPIC, DFT CALCULATION, MOLECULAR DOCKING AND MOLECULAR DYNAMIC SIMULATIONS., Studia Universitatis Babes-Bolyai, Chemia 70 (2025).

[36] S. Khamouli, S. Belaidi, T. Lanez, Molecular doking and ADMET studies of amino-pyrimidine derivaties as mycobacterium tuberculosis Ser/Thr protein kinases B inhibitors, Journal of Fundamental and Applied Sciences 11 (2019) 914–939.

[37] H. Mouada, T. Lanez, I. Zafar, ROS scavenging, DNA binding and NADPH oxidase inhibition potential of N'-Ferrocenylmethyl-N'-phenylpropionohydrazide using cyclic voltammetry and molecular docking, J. Organomet. Chem. 1007 (2024) 123026.

[38] T. Lanez, M. Henni, H. Hemmami, Development of cyclic voltammetric method for the study of the interaction of antioxidant standards with superoxide anion radicals case of α-tocopherol, Scientific Study and Research: Chemistry and Chemical Engineering, Biotechnology, Food Industry 16 (2015) 161–168.

[39] Y. Bekkar, E. Lanez, T. Lanez, L. Bourougaa, A. Adaika, Z. Saada, A. Benine, Antidiabetic Potential of Synthesized Ferrocenylmethylaniline Derivatives: Insights From In Vitro Studies, Molecular Docking, ADMET, DFT Calculations, and Molecular Dynamics Simulation, Biotechnol. Appl. Biochem. (2025).

[40] Y. Bekkar, E. Lanez, T. Lanez, L. Bourougaa, A. Adaika, A. Benine, Z. Saada, Combined In Vitro and In Silico analysis of ferrocenylmethylaniline derivatives: Antibacterial potential, DFT calculations, and molecular dynamics insights, J. Organomet. Chem. (2025) 123618.

[41] E. Lanez, L. Zerrouk, L. Bechki, T. Lanez, A. Adaika, N. Zegheb, K. Nesba, Synthesis, molecular docking, drug-likeness analysis, and ADMET prediction of nickel and zinc tetraphenyl-porphyrin complexes as possible antioxidant agents, Journal of the Chinese Chemical Society (n.d.).

[42] S.N. Nacer, T. Lanez, Electrochemical properties of N'-ferrocenylmethyl-N'-phenylbenzohydrazide in aqueous and organic mediums, International Letters of Chemistry, Physics and Astronomy 5 (2013) 76–85.

[43] H. Laraoui, E. Lanez, N. Zegheb, A. Adaika, T. Lanez, M. Benkhaled, Anti-Diabetic Activity of Flavonol Glucosides From Fumana montana Pomel: In vitro Analysis, In Silico Docking, ADMET Prediction, and Molecular Dynamics Simulations, ChemistrySelect 8 (2023) e202204512. https://doi.org/10.1002/slct.202204512.

[44] T. Lanez, M. Henni, Dual Anti-Inflammatory and Antidiabetic Potential of Ferrocenylmethylcyanophenyl Derivatives: Integrated In Vitro and In Silico Evaluation, J. Organomet. Chem. (2025) 123956.

[45] A. Khelef, T. Lanez, In vitro assays of the antioxidant activities of ferrocene derivatives bearing amine, amide or hydrazine groups, . 7 (2015) 318–323.

[46] T. Zaiz, T. Lanez, Corrosion inhibition of carbon steel XC70 in H_2SO_4 solution by ferrocene derivative 3-(ferrocenylmethylamine)benzonitrile, Journal of Fundamental and Applied Sciences 4 (2015) 182. https://doi.org/10.4314/jfas.v4i2.8.

[47] T. Lanez, H. Hemmami, Antioxidant Activities of N-ferrocenylmethyl-2- and -3-nitroaniline and Determination of their Binding Parameters with Superoxide Anion Radicals, Curr. Pharm. Anal. 13 (2016) 110–116. https://doi.org/10.2174/1573412912666160831145524.

[48] N. Benyza, F. Allouche, S.W. Dammak, E. Lanez, T. Lanez, Chemical Reactivity, Topological Analysis, and Second-Order Nonlinear Optical Responses of M3O@ Al12N12: A Quantum Chemical Study, Russian Journal of Physical Chemistry A 96 (2022) 2909–2920.

[49] E. Lanez, A. Kedadra, T. Lanez, A. Adaika, N. Zegheb, In vitro antioxidant activity, QSAR, in silico toxicity prediction, molecular docking studies, and molecular dynamics of a series of N-ferrocenylmethylanilines as potent antioxidant agents, J. Organomet. Chem. (2024) 123284.

[50] C. Filote, E. Lanez, V.I. Popa, T. Lanez, I. Volf, Characterization and Bioactivity of Polysaccharides Separated through a (Sequential) Biorefinery Process from Fucus spiralis Brown Macroalgae, Polymers (Basel). 14 (2022) 4106. https://doi.org/10.3390/polym14194106.

[51] A. Boutarfaia, L. Bechki, T. Lanez, E. Lanez, M. Kadri, Synthesis, Antioxidant Activity, and Determination of Binding Parameters of Meso-Tetra-4-Actophenyl-Porphyrin and its Palladium (II) Complex with Superoxide Anion Radicals, Curr. Bioact. Compd. 16 (2019) 1063–1071. https://doi.org/10.2174/1573407215666191017105239.

[52] A. Yahiaoui, N. Benyza, A. Messai, T. Lanez, E. Lanez, Voltametric and molecular docking investigations of ferrocenylmethylaniline and its N-acetylated derivative interacting with DNA, Journal of Electrochemical Science and Engineering (2023). https://doi.org/10.5599/jese.2061.

[53] A. Kedadra, T. Lanez, E. Lanez, H. Hemmami, M. Henni, Synthesis and antioxidant activity of six novel N-ferrocenylmethyl-N-(nitrophenyl)and-N-(cyanophenyl)-acetamides: Cyclic voltammetry and molecular docking studies, Journal of Electrochemical Science and Engineering 12 (2022) 293–304. https://doi.org/10.5599/jese.1162.

[54] A. Khennoufa, L. Bechki, T. Lanez, E. Lanez, N. Zegheb, Spectrophotometric, voltammetric and molecular docking studies of binding interaction of N-ferrocenylmethylnitroanilines with bovine serum albumin, J. Mol. Struct. 1224 (2021) 129052. https://doi.org/10.1016/j.molstruc.2020.129052.

[55] M. Meraghni, T. Lanez, E. Lanez, L. Bechki, A. Kennoufa, Experimental and theoretical study on corrosion inhibition of mild steel by meso-tetraphenyl-porphyrin derivatives in acid solution, Journal of Electrochemical Science and Engineering 13 (2023) 217–229. https://doi.org/10.5599/jese.1400.

[56] T. Lanez, M. Feizi-Dehnayebi, E. Lanez, Assessment of the electrostatic binding of ferrocenylmethyl-nitroaniline derivatives to DNA: A combined experimental and theoretical study, J. Mol. Struct. (2024) 138386.

[57] Z. Nadjiba, B. Chérifa, T. Lanez, E. Lanez, In Silico Study on N-ferrocenylmethyl-N-phenylpropionohydrazide and N-ferrocenylmethyl-N-pheylbenzohydrazide as anticancer drugs for breast and prostate cancer, International Journal of Pharmacology, Phytochemistry and Ethnomedicine 11 (2018) 17–25.

[58] L. ZERROUK, L. BECHKI, E. LANEZ, T. LANEZ, Synthesis, characterization, cyclic voltammetry, and molecular docking studies of the antioxidant activities of superoxide anion radicals towards meso-tetramethophenyl-porphyrin and meso-tetrabiphenyl-porphyrin, Not. Sci. Biol. 16 (2024) 11823. https://doi.org/10.55779/nsb16211823.

[59] A. Adaika, A. Adaika, T. Lanez, E. Lanez, in Vitro and in Silico Evaluation of Anticancer Activity of N,N-Dimethylaminomethylferrocene, Journal of Fundamental and Applied Sciences 11 (2019) 748–768. https://jfas.info/index.php/JFAS/article/view/289.

[60] T. Lanez, H. Benaicha, E. Lanez, M. Saidi, Electrochemical, spectroscopic and molecular docking studies of 4-methyl-5-((phenylimino)methyl)-3H- and 5-(4-fluorophenyl)-3H-1,2-dithiole-3-thione interacting with DNA, Journal of Sulfur Chemistry 39 (2018) 76–88. https://doi.org/10.1080/17415993.2017.1391811.

[61] N. ZEGHEB, L. Elhafnaoui, T. Lanez, N-ferrocenylmethyl-derivatives as spike glycoprotein inhibitors of sars-cov-2 using in silico approaches, (2020).

[62] E. Lanez, T. Lanez, N. Zegheb, In silico ADMET, toxicological analysis, molecular docking studies and Molecular dynamics simulation of Afzelin with potential antibacterial effects against Staphylococcus aureus, Turkish Computational and Theoretical Chemistry 7 (2023) 10–16.

[63] H. Mouada, T. Lanez, E. Lanez, Investigations of the binding parametres of the interaction of N'-ferrocenylmethyl-N'-phenylaceto-and propionohydrazide with DNA, Journal of Fundamental and Applied Sciences 11 (2019) 875–882.

[64] E. Lanez, L. Bechki, T. Lanez, Computational molecular docking, voltammetric and spectroscopic DNA interaction studies of 9N-(Ferrocenylmethyl)adenine, Chemistry and Chemical Technology 13 (2019) 11–17. https://doi.org/10.23939/chcht13.01.011.

[65] T. Lanez, E. Lanez, A molecular docking study of N-ferrocenylmethylnitroanilines as potential anticancer drugs, International Journal of Pharmacology, Phytochemistry and Ethnomedicine 2 (2016) 5–12.

[66] L. Guan, H. Yang, Y. Cai, L. Sun, P. Di, W. Li, G. Liu, Y. Tang, ADMET-score-a comprehensive scoring function for evaluation of chemical drug-likeness, Medchemcomm 10 (2019) 148–157. https://doi.org/10.1039/C8MD00472B.

[67] G. Xiong, Z. Wu, J. Yi, L. Fu, Z. Yang, C. Hsieh, M. Yin, X. Zeng, C. Wu, A. Lu, ADMETlab 2.0: an integrated online platform for accurate and comprehensive predictions of ADMET properties, Nucleic Acids Res. 49 (2021) W5–W14.

[68] D. Dascalu, D. Larisa Roman, M. Filip, A. Ciorsac, V. Ostafe, A. Isvoran, Solubility and Admet Profiles of Short Oligomers of Lactic Acid, ADMET DMPK 8 (2020) 425–436. https://doi.org/10.5599/admet.801.

[69] J. Hodgson, ADMET—turning chemicals into drugs, Nat. Biotechnol. 19 (2001) 722–726.